

# Modeling the *cis*-Oxo-Labile Binding Site Motif of Non-Heme Iron Oxygenases: Water Exchange and Oxidation Reactivity of a Non-Heme Iron(IV)-Oxo Compound Bearing a Tripodal Tetradentate Ligand

Anna Company,<sup>[a, e]</sup> Irene Prat,<sup>[a]</sup> Jonathan R. Frisch,<sup>[b]</sup> Dr Ruben Mas-Ballesté,<sup>[b]</sup> Mireia Güell,<sup>[c]</sup> Gergely Juhász,<sup>[d]</sup> Xavi Ribas,<sup>[a]</sup> Dr Eckard Münck,<sup>\*,[d]</sup> Josep M. Luis,<sup>\*,[c]</sup> Lawrence Que, Jr.,<sup>\*,[b]</sup> and Miquel Costas<sup>\*,[a]</sup>

**Abstract:** The spectroscopic and chemical characterization of a new synthetic non-heme iron(IV)-oxo species  $[\text{Fe}^{\text{IV}}(\text{O})(^{\text{Me,H}}\text{Pytacn})(\text{S})]^{2+}$  (**2**,  $^{\text{Me,H}}\text{Pytacn} = 1-(2'\text{-pyridylmethyl})-4,7\text{-dimethyl-1,4,7-triazacyclononane}$ ,  $\text{S} = \text{CH}_3\text{CN}$  or  $\text{H}_2\text{O}$ ) is described. Complex **2** was prepared by reaction of  $[\text{Fe}^{\text{II}}(\text{CF}_3\text{SO}_3)_2(^{\text{Me,H}}\text{Pytacn})]$  (**1**) with peracetic acid. Complex **2** bears a tetradentate  $\text{N}_4$  ligand that leaves two *cis* sites available for binding an oxo group and

a second external ligand but, unlike the related iron(IV)-oxo species with tetradentate ligands, it is remarkably stable at room temperature ( $t_{1/2} > 2$  h at 288 K). Its ability to exchange the oxygen atom of the oxo ligand with water has been analyzed in detail by

**Keywords:** bioinorganic chemistry • iron • oxygenases • reaction mechanisms • tetradentate ligands

means of kinetic studies, and a mechanism is proposed on the basis of DFT calculations. Hydrogen-atom abstraction from C–H bonds and oxygen-atom transfer to sulfides by **2** have also been studied. Despite its thermal stability, **2** proves to be a very powerful oxidant that is capable of breaking the strong C–H bond of cyclohexane (bond dissociation energy = 99.3 kcal mol<sup>-1</sup>).

[a] Dr. A. Company, I. Prat, Dr. X. Ribas, Dr. M. Costas  
Departament de Química  
Universitat de Girona  
Campus Montilivi, E17071 Girona, Catalonia (Spain)  
Fax: (+34) 972-41-81-50  
E-mail: miquel.costas@udg.edu

[b] J. R. Frisch, D. R. Mas-Ballesté, Prof. Dr. L. Que, Jr.  
Department of Chemistry and Center for Metals in Biocatalysis  
University of Minnesota  
Minneapolis, MN 55455 (USA)  
Fax: (+1) 612-625-0389  
E-mail: larryque@umn.edu

[c] Dr. M. Güell, Dr. J. M. Luis  
Institut de Química Computacional  
Universitat de Girona  
Campus Montilivi, E17071 Girona, Catalonia (Spain)  
Fax: (+34) 972-41-83-56  
E-mail: josepm.luis@udg.edu

[d] Dr. G. Juhász, Prof. D. E. Münck  
Department of Chemistry  
Carnegie Mellon University  
4400 Fifth Avenue, Pittsburgh, PA 15213 (USA)  
Fax: (+1) 412-268-5058  
E-mail: em40@andrew.cmu.edu

[e] Dr. A. Company  
Present address: Institut für Chemie, Technische Universität  
Berlin (Germany)

Supporting information for this article is available on the WWW under <http://dx.doi.org/10.1002/chem.201002297>.

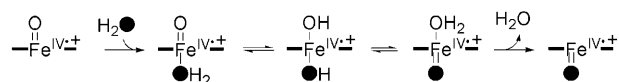
## Introduction

Iron(IV)-oxo compounds are proposed as the active species in the catalytic cycles of several  $\text{O}_2$ -activating non-heme iron enzymes, such as isopenicillin N-synthase, pterin-dependent hydroxylases, and 2-oxoglutarate-dependent oxygenases.<sup>[1–3]</sup> Quite recently, high-spin ( $S=2$ ) iron(IV)-oxo intermediates have been trapped and spectroscopically characterized in five different non-heme iron enzymes: namely, taurine: $\alpha$ -ketoglutarate dioxygenase (TauD),<sup>[4,5]</sup> halogenase CytC3,<sup>[6]</sup> propyl-4-hydroxylase,<sup>[7]</sup> tyrosine hydroxylase,<sup>[8]</sup> and aliphatic halogenase, SyrB2.<sup>[9]</sup> Parallel synthetic efforts have succeeded in the preparation of octahedral  $S=2$   $[\text{Fe}^{\text{IV}}(\text{O})(\text{H}_2\text{O})_5]^{2+}$ <sup>[10]</sup> and octahedral  $S=1$   $\text{Fe}^{\text{IV}}=\text{O}$  species using tetradentate  $\text{N}_4$  ligands with available *trans*-binding sites,<sup>[11,12]</sup> tetradentate  $\text{N}_4$  ligands with available *cis*-binding sites,<sup>[13–17]</sup> pentadentate  $\text{N}_5$  ligands,<sup>[18–22]</sup> and a pentadentate  $\text{N}_4\text{S}$  ligand.<sup>[23]</sup> Very recently, two examples of trigonal bipyramidal  $S=2$  iron(IV)-oxo complexes, which bear structural and electronic resemblance to the enzymatic non-heme intermediates, have been described.<sup>[24–26]</sup>

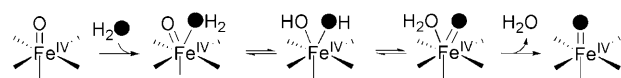
These metastable and highly oxidizing complexes have been characterized by various spectroscopic techniques including, in selected cases, X-ray crystallography.<sup>[11,22,25–27]</sup> The ability of synthetic non-heme  $\text{Fe}^{\text{IV}}(\text{O})$  species to act as

oxidants has been proved<sup>[28,29]</sup> and several studies demonstrate that they are capable of performing several oxidation reactions including: oxygen-atom transfer to sulfides and triphenylphosphine,<sup>[16,30,31]</sup> epoxidation<sup>[13,19,21]</sup> and possible dihydroxylation<sup>[21,32]</sup> of alkenes, alcohol oxidation,<sup>[33]</sup> hydrogen-atom abstraction,<sup>[18,34,35]</sup> aliphatic and aromatic hydroxylation,<sup>[36,37]</sup> oxo transfer to other Fe<sup>II</sup> complexes,<sup>[38]</sup> and glutathione and peptide oxidation.<sup>[39,40]</sup> On the other hand, by analogy to the better studied heme systems,<sup>[41]</sup> it is widely postulated that non-heme iron-oxo species can exchange their oxygen atom with water through an oxo-hydroxo tautomerism before attack to a substrate (Scheme 1). Thus, in-

heme systems



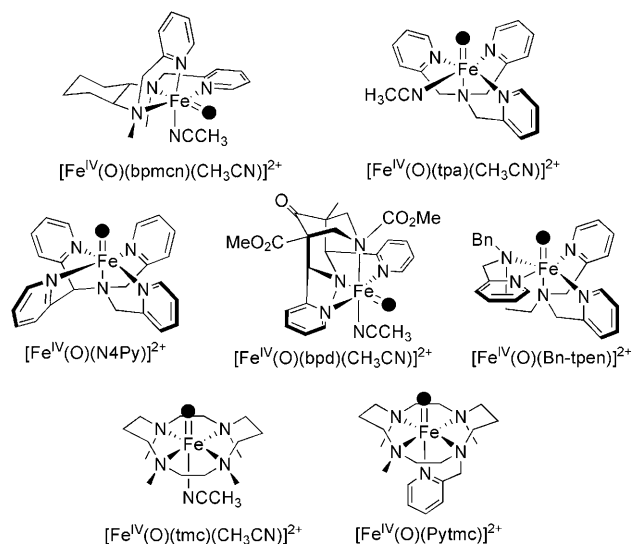
non-heme iron models: tmc and N4Py



Scheme 1. Top: Proposed oxo-hydroxo tautomerism in heme systems. Bottom: Proposed oxo-hydroxo tautomerism in  $[\text{Fe}^{\text{IV}}(\text{O})(\text{tmc})(\text{CH}_3\text{CN})]^{2+}$  ( $\text{tmc} = 1,4,8,11\text{-tetraaza-cyclotetradecane}$ ) and  $[\text{Fe}^{\text{IV}}(\text{O})(\text{N4Py})]^{2+}$  ( $\text{N4Py} = N,N\text{-bis}(2\text{-pyridylmethyl})\text{-}N\text{-bis}(2\text{-pyridyl})\text{methylamine}$ ).

direct evidence for the participation of these compounds in the catalytic cycle of enzymes<sup>[42]</sup> and/or synthetic models<sup>[43]</sup> comes from the incorporation of oxygen from water into oxidized products. Recently, this has been experimentally proved in two synthetic non-heme iron(IV)-oxo species; well-defined  $[\text{Fe}^{\text{IV}}(\text{O})(\text{tmc})(\text{CH}_3\text{CN})]^{2+}$  and  $[\text{Fe}^{\text{IV}}(\text{O})(\text{N4Py})]^{2+}$  (Scheme 2) have been shown to undergo exchange with water (Scheme 1).<sup>[44]</sup>

Because the vast majority of non-heme iron oxygenases contain *cis*-labile binding sites, synthetic iron(IV)-oxo complexes with tripodal tetradentate ligands are especially relevant from a biological point of view. However, they have proved to be less stable than their pentadentate counterparts,<sup>[28]</sup> thus rendering their study more difficult. For this reason most of the studies have been performed by using pentadentate N<sub>5</sub> ligands (N4Py) or equatorial tetradentate N<sub>4</sub> ligands with two labile sites in a *trans* configuration (tmc). Herein, we address this issue and we describe the preparation and spectroscopic and chemical characterization of a new Fe<sup>IV</sup>(O) species bearing the tripodal tetradentate 1-(2'-pyridylmethyl)-4,7-dimethyl-1,4,7-triazacyclononane ligand (<sup>Me,H</sup>Pytacn). This species shows an unprecedented high stability at room temperature, which allows us to evaluate several biologically relevant aspects of its reactivity. These studies include the evaluation of its ability to perform oxygen-atom transfer to sulfides and

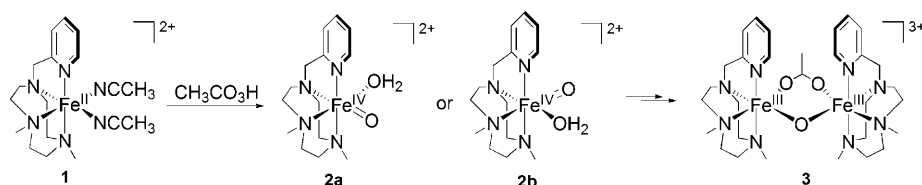


Scheme 2. Schematic representation of synthetic Fe<sup>IV</sup>(O) complexes relevant to this work. bpmcn = *N,N'*-bis(2-pyridylmethyl)-*N,N'*-dimethyl-*trans*-1,2-diaminocyclohexane, tpa = tris(2-pyridylmethyl)amine, bpd = dimethyl 2,4-bis(2-pyridinyl)-3,7-diazabicyclo-[3.3.1]nonane-9-on-1,5-dicarboxylate, Bn-tpen = *N*-benzyl-*N,N',N'*-tris(2-pyridylmethyl)-1,2-diaminoethane, Pytmc = 1-(2'-pyridylmethyl)-4,8,11-Tetramethyl-1,4,8,11-tetraaza-cyclotetradecane.

hydrogen-atom abstraction reactions. Moreover, the exchange of its oxo group with the oxygen atom from H<sub>2</sub><sup>18</sup>O has been studied by means of kinetic and computational methods.

## Results and Discussion

**Preparation and characterization of the Fe<sup>IV</sup>(O) species:** Reaction of  $[\text{Fe}^{\text{II}}(\text{CF}_3\text{SO}_3)_2(\text{Me,HPytacn})]$  (**1**; Scheme 3)<sup>[45]</sup> with two equivalents of peracetic acid (CH<sub>3</sub>CO<sub>3</sub>H) in CH<sub>3</sub>CN at 15 °C produces, within 20 min, a novel species (**2**) with a UV/Vis spectrum showing a band at  $\lambda_{\text{max}} = 750 \text{ nm}$  ( $\epsilon = 200 \text{ M}^{-1} \text{ cm}^{-1}$ ) and a weaker shoulder around 900 nm ( $\epsilon \approx 100 \text{ M}^{-1} \text{ cm}^{-1}$ ; Figure 1). Complex **2** is relatively stable in solution, with a half-life time ( $t_{1/2}$ ) of 2.4 h at 15 °C. The nature of the transient species **2** has been determined by a combination of Mössbauer, <sup>1</sup>H NMR, and resonance Raman spectroscopy, ESI-MS, and DFT calculations. We studied the Mössbauer spectra of **2** in acetonitrile between 4.2 and 100 K in parallel applied magnetic fields up to 8.0 T. Two representative spectra are shown in Figure 2. In zero applied



Scheme 3. Schematic view of formation and decay of **2**, along with the proposed chemical structures of **1–3**.

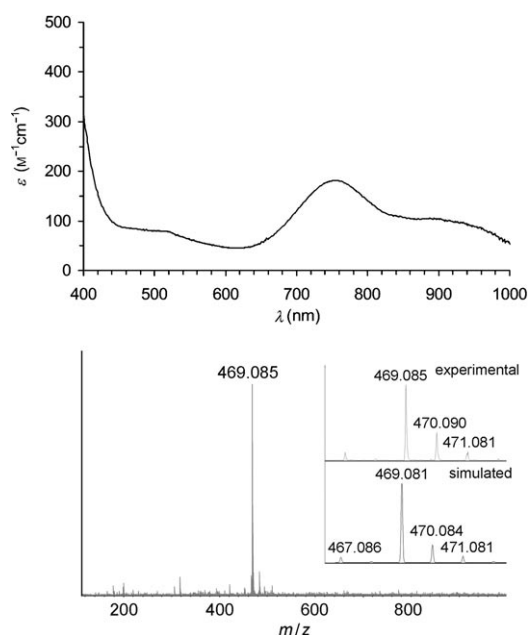


Figure 1. UV/Vis spectrum of **2** (top) and its ESI mass spectrum (bottom).

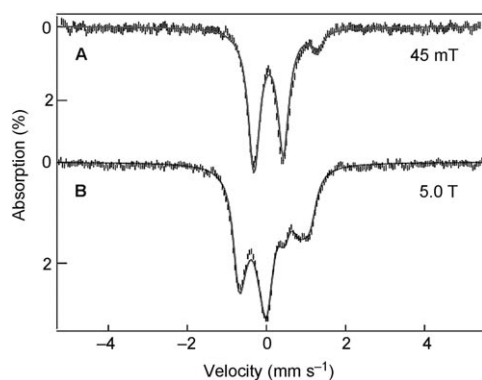


Figure 2. Mössbauer spectrum of **2** in acetonitrile, recorded at 4.2 K in a parallel field as indicated. Solid lines are spectral simulations based on an  $S=1$  spin Hamiltonian<sup>[23]</sup> with the zero-field splitting parameters  $D=+27\text{ cm}^{-1}$ ,  $E/D=0$ ,  $^{57}\text{Fe}$  magnetic hyperfine tensor  $A_{x,y,z}/g_{\mu}\beta=(-23.7, -20.5, -4.5)\text{ T}$ , quadrupole parameters  $\Delta E_{\text{O}}=0.73\text{ mm s}^{-1}$ ,  $\eta=1$ , and isomer shift  $\delta=0.05\text{ mm s}^{-1}$ .

magnetic field (Figure 2A), **2** exhibits at 4.2 K a quadrupole doublet, which represents 85(5)% of the total iron, with quadrupole splitting  $\Delta E_{\text{O}}=0.73\text{ mm s}^{-1}$  and isomer shift  $\delta=0.05\text{ mm s}^{-1}$ . These parameters, together with the fact that **2** has integer electron spin (as witnessed by the observation that **2** displays a doublet rather than magnetically split spectra in zero field), show that **2** is an  $\text{Fe}^{\text{IV}}$  complex. Spectra recorded in applied magnetic fields (see, e.g., Figure 2B) have features very similar to those reported for  $S=1$   $\text{Fe}^{\text{IV}}(\text{O})$  complexes;  $S=2$   $\text{Fe}^{\text{IV}}(\text{O})$  complexes display quite different spectra.<sup>[6,8,10,24]</sup> We analyzed the spectra of **2** with the commonly used  $S=1$  spin Hamiltonian,<sup>[23]</sup> the parameters obtained are very similar to those obtained for other  $S=1$   $\text{Fe}^{\text{IV}}(\text{O})$  complexes and are listed in the caption of Figure 2.

The spectrum of Figure 2A indicates the presence of an  $S=0$  diferric contaminant with  $\Delta E_{\text{O}}=1.60\text{ mm s}^{-1}$  and  $\delta=0.45\text{ mm s}^{-1}$ , which represents approximately 15% of Fe. For the present chemistry such complexes are decomposition products that frequently represent the thermodynamic sink.<sup>[13]</sup>

High-resolution ESI-MS establishes the elemental composition of **2** (Figure 1, bottom) as it reveals a clean spectrum with a major peak with a mass value at  $m/z$  469.08 and an isotopic pattern fully consistent with the ion  $\{[\text{Fe}^{\text{IV}}(\text{O})(\text{CF}_3\text{SO}_3)(^{\text{Me,H}}\text{Pytacn})]\}^+$ . Evidence for the presence of the oxo ligand was provided by vibrational spectroscopy. Resonance Raman analysis on frozen acetonitrile solutions of **2** with laser excitation at  $\lambda_{\text{exc}}=407.9\text{ nm}$  shows a resonance-enhanced feature at  $831\text{ cm}^{-1}$  that downshifts to  $788\text{ cm}^{-1}$  when **2** is allowed to react with  $\text{H}_2^{18}\text{O}$ . The energy of the band falls in the range of reported synthetic<sup>[11,15,22,24,46]</sup> and enzymatic<sup>[47]</sup> non-heme  $\text{Fe}=\text{O}$  stretching vibrations, and the  $-43\text{ cm}^{-1}$  shift is in reasonable agreement with the shift of  $-37\text{ cm}^{-1}$  predicted by Hooke's law for a diatomic  $\text{Fe}-\text{O}$  stretch and  $-40\text{ cm}^{-1}$  predicted by DFT calculations.<sup>[48,49]</sup> In conclusion, the spectroscopic data allow us to formulate **2** as a new iron(IV)-oxo species  $[\text{Fe}^{\text{IV}}(\text{O})(^{\text{Me,H}}\text{Pytacn})(\text{S})]^{2+}$ , where solvent  $\text{S}=\text{CH}_3\text{CN}$  or  $\text{H}_2\text{O}$ . The nature of the sixth ligand could not be experimentally determined, but insight into its nature can be obtained from the DFT calculations described in the next section. Acetonitrile binding was previously documented in the crystallographic characterization of  $[\text{Fe}^{\text{IV}}(\text{O})(\text{tmc})(\text{CH}_3\text{CN})]^{2+}$ .<sup>[11]</sup> However, in the present case, the presence of a water ligand is proposed on the basis of DFT calculations (see below), which indicated that these species are thermodynamically more stable than the corresponding analogue containing an acetonitrile ligand.<sup>[13,14]</sup>

Because of the inequivalence of the two binding positions not occupied by  $^{\text{Me,H}}\text{Pytacn}$ , two isomeric forms are possible for **2** (**2a** and **2b**, Scheme 3). These two isomers differ not only in the group disposed *trans* to the oxo ligand but also in the relative orientation of the pyridine ring with respect to the  $\text{Fe}-\text{O}$  axis. However, the  $^1\text{H}$  NMR spectrum of **2** (Figure 3) showed a unique set of sharp signals that could be assigned to the pyridine  $\beta$  (42 ppm),  $\gamma$  (10 ppm), and  $\beta'$  ( $-13\text{ ppm}$ ) protons. The shift pattern for these signals is reminiscent of that found in the  $^1\text{H}$  NMR spectrum of

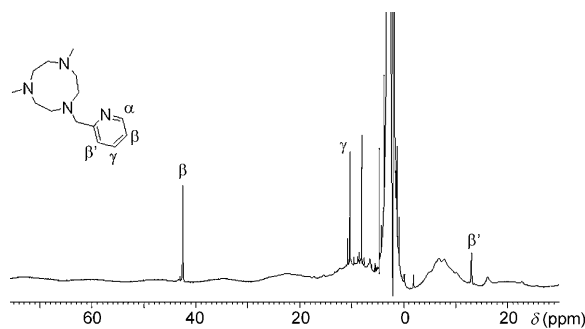


Figure 3.  $^1\text{H}$  NMR spectrum of **2** at 298 K in  $\text{CD}_3\text{CN}$ , along with selected signal identifications.

$[\text{Fe}^{\text{IV}}(\text{O})(\text{N4Py})]^{2+}$ , in which all four pyridine rings are disposed parallel to the Fe–O axis, and different from the pattern associated with pyridine rings oriented perpendicular to the Fe=O axis.<sup>[27]</sup> Thus, in the present case, the NMR spectrum indicates that only isomer **2a** is present in solution, with the pyridine ring disposed parallel to the Fe–O axis.

Despite the inherently low stability of high-valent oxo-iron(IV) species, the <sup>1</sup>H NMR spectrum of **2** lacks signals corresponding to **1**<sup>[50]</sup> and **3** (the dinuclear Fe<sup>III</sup> decomposition product, see below and the Supporting Information), thus suggesting that **2** is prepared with good purity, in accordance with the Mössbauer analysis (see above).

**DFT analysis of the structures of the two isomers of 2:** DFT calculations were employed to help clarify the molecular and electronic structure of **2**.<sup>[48,49]</sup> The nature of the sixth ligand that completes the octahedral coordination sphere of the iron center was first studied by comparing the relative energies of the corresponding  $[\text{Fe}^{\text{IV}}(\text{O})(\text{Me,HPytacn})(\text{S})]^{2+}$  ( $\text{S}=\text{CH}_3\text{CN}$  and  $\text{H}_2\text{O}$ ) complexes. Computational analysis for  $\text{S}=\text{H}_2\text{O}$  indicates that hydrogen bonding between the water ligand and a second, external water molecule is very strong because of the dicationic nature of **2**. This interaction stabilizes  $[\text{Fe}^{\text{IV}}(\text{O})(\text{Me,HPytacn})(\text{H}_2\text{O})]^{2+}$  relative to  $[\text{Fe}^{\text{IV}}(\text{O})(\text{Me,HPytacn})(\text{CH}_3\text{CN})]^{2+}$  by  $\Delta G=16.1$  kcal mol<sup>-1</sup>. Acetonitrile binding has been previously demonstrated in the X-ray structure of  $[\text{Fe}^{\text{IV}}(\text{O})(\text{tmc})(\text{CH}_3\text{CN})]^{2+}$ ,<sup>[11]</sup> for which the hydrophobic pocket created by the N-Me groups of tmc isolates the acetonitrile ligand. This is likely to prevent intermolecular interactions with additional water molecules. In contrast, the tripodal tetradentate Me,HPytacn ligand lacks such a sterically restricted hydrophobic pocket, which may constitute the key structural feature that favors water binding over acetonitrile in **2**.

Optimized molecular structures of  $[\text{Fe}^{\text{IV}}(\text{O})(\text{Me,HPytacn})(\text{H}_2\text{O})]^{2+}$  (**2a** and **2b**) obtained by DFT calculations are shown in Figure 4, with selected structural parameters given in the caption.<sup>[51]</sup> The relative DFT energies of the two isomeric forms of **2** indicate that **2a** is energetically favored by 2.1 kcal mol<sup>-1</sup>, thus supporting our structural assignment based on NMR spectroscopy. Energies corresponding to singlet ( $S=0$ ) and quintet states ( $S=2$ ) of **2a** and **2b** were also

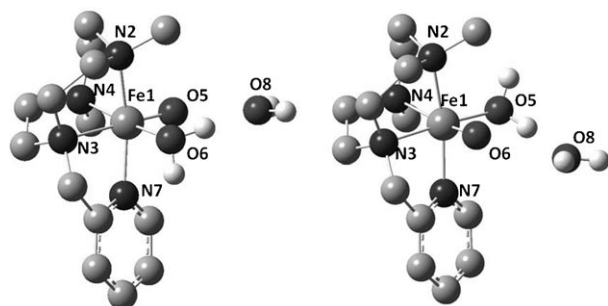


Figure 4. DFT-calculated structures of **2a** (left) and **2b** (right). Selected bond lengths [Å] for **2a**: Fe1–N2 2.05, Fe1–N3 2.11, Fe1–N4 2.06, Fe1–O5 2.06, Fe1–O6 1.62, Fe1–N7 2.03 and **2b**: Fe1–N2 2.07, Fe1–N3 1.99, Fe1–N4 2.19, Fe1–O5 1.63, Fe1–O6 2.03, Fe1–N7 2.02.

computed (Table S7 in the Supporting Information). The substantially higher energies of these states, when compared with the triplet ( $S=1$ ) state, further support the Mössbauer-based spin-state assignment of **2**. Structural parameters for **2a** and **2b** are very similar. The computed Fe–O distances in **2a** and **2b** are 1.62 and 1.63 Å, respectively, in good agreement with structurally characterized examples of synthetic<sup>[11,17,22,24–27,52]</sup> and enzymatic<sup>[53,54]</sup> non-heme iron(IV)-oxo species. The oxo ligand exerts a *trans* effect that is indicated by a  $\approx 0.1$  Å lengthening of the corresponding *trans* Fe–N distance (compare  $d_{\text{Fe1–N4}}=2.19$  Å in **2b** with 2.06 Å in **2a**, and  $d_{\text{Fe1–N3}}=1.99$  Å in **2b** with 2.11 Å in **2a**). The Fe–N<sub>py</sub> distance is 2.03 Å in **2a** and 2.02 Å in **2b**, values that appear somewhat intermediate between the short  $d_{\text{Fe–Npy}} \approx 1.95$  Å of the pyridine rings *cis* to the oxo ligand in  $[\text{Fe}^{\text{IV}}(\text{O})(\text{N4Py})](\text{ClO}_4)_2$ <sup>[27]</sup> and the longer  $d_{\text{Fe–Npy}}=2.118(3)$  Å of  $[\text{Fe}^{\text{IV}}(\text{O})(\text{Pytmc})](\text{CF}_3\text{SO}_3)_2$ <sup>[22]</sup> for which the pyridine is bound *trans* to the oxo ligand.

**Relative thermal stability and decay of 2:**  $[\text{Fe}^{\text{IV}}(\text{O})(\text{Me,HPytacn})(\text{S})]^{2+}$  (**2**) joins the growing family of iron(IV)-oxo species formed with tetradentate ligands tmc,<sup>[11]</sup> tpa,<sup>[16]</sup> N,N', dimethyl-*N,N'*-bis(8-quinolyl)ethane-1,2-diamine (bqen),<sup>[17]</sup> bpd,<sup>[35]</sup> and bpmcn<sup>[14]</sup> (Scheme 2). In the case of tmc, the ligand topology gives rise to an iron center with two available *trans* sites, one of which is occupied by an oxo ligand in the Fe<sup>IV</sup>-oxo compound. Instead, ligands such as Me,HPytacn, tpa, bpd, bqen, and bpmcn wrap around the metal ion, so that two sites in a *cis* relative disposition are ready for interaction with exogenous ligands. Thus, in the corresponding iron(IV)-oxo compounds, the oxo group binds to one of these positions and the other site is presumably occupied by a neutral labile molecule, such as acetonitrile or water (Scheme 2). Despite the similar coordination spheres around the metal center, the resulting iron(IV)-oxo compounds exhibit remarkably different stabilities.  $[\text{Fe}^{\text{IV}}(\text{O})(\text{bpmcn})(\text{S})]^{2+}$ ,  $[\text{Fe}^{\text{IV}}(\text{O})(\text{tpa})(\text{S})]^{2+}$ , and  $[\text{Fe}^{\text{IV}}(\text{O})(\text{bpd})(\text{S})]^{2+}$  ( $\text{S}=\text{CH}_3\text{CN}$  or  $\text{H}_2\text{O}$ ) can only be prepared in good yields at  $-40^\circ\text{C}$  because they easily decompose at higher temperatures.<sup>[13,14,35]</sup>  $[\text{Fe}^{\text{IV}}(\text{O})(\text{bqen})(\text{S})]^{2+}$  has a lifetime of  $t_{1/2} \approx 30$  min at  $0^\circ\text{C}$ .<sup>[17]</sup> In contrast, **2** can be generated and remains relatively stable at  $15^\circ\text{C}$ .

Thermal decay of **2** leads to a new species **3** that has been identified as  $[\text{Fe}^{\text{III}}_2(\mu\text{-O})(\mu\text{-CH}_3\text{CO}_2)(\text{Me,HPytacn})_2]^{3+}$  by means of UV/Vis spectroscopy, ESI-MS, and comparison with an independently prepared sample characterized by X-ray crystallography (Figure 5).<sup>[55]</sup> The relatively poor stability observed for iron(IV)-oxo species with tripodal tetradentate ligands, in comparison with those that contain pentadentate or tetradentate ligands with *trans* topologies, can be understood by considering that only the latter two offer effective steric protection of the oxo ligand against decomposition into a diiron complex. In addition, these “stable” iron(IV) compounds lack a *cis*-labile site adjacent to the reactive oxo ligand, thus precluding prebinding of a putative substrate. Based on these arguments, we suggest that the surprising thermal stability of **2** derives from a combination

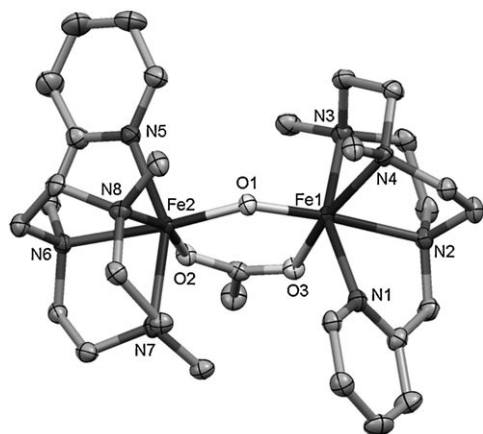


Figure 5. ORTEP plot (50% probability ellipsoids) of  $[\text{Fe}^{\text{III}}_2(\mu\text{-O})(\mu\text{-CH}_3\text{CO}_2)(\text{Me,H-Pytcn})_2](\text{ClO}_4)_3 \cdot \text{CH}_3\text{CN}$  ( $\mathbf{3} \cdot \text{CH}_3\text{CN}$ ). Selected bond lengths [Å] and angles [°]: Fe1–O1 1.801(3), Fe1–O3 2.062(4), Fe1–N1 2.167(4), Fe1–N3 2.180(4), Fe1–N4 2.197(4), Fe1–N2 2.225(4), O1–Fe2 1.805(3), Fe2–O2 2.017(3), Fe2–N5 2.163(4), Fe2–N8 2.184(4), Fe2–N7 2.196(4), Fe2–N6 2.247(4); O1–Fe1–O3 95.42(15), Fe2–O1–Fe1 135.2(2).

of the oxidatively robust nature of the  $\text{Me,H-Pytcn}$  ligand and some steric hindrance imposed by the N-Me groups of the ligand that project into the space surrounding the Fe=O unit. Consistent with this notion, in the absence of acetate ion, which facilitates dimerization, the oxidation of **1** with  $\text{H}_2\text{O}_2$  in an aqueous acetonitrile solvent mixture does not result in the common rapid formation of oxo-bridged ferric dimers,<sup>[56]</sup> but instead in the formation of the mononuclear species formulated as  $[\{\text{Fe}^{\text{III}}(\text{OH})(\text{Me,H-Pytcn})\}(\text{CF}_3\text{SO}_3)]^+$  on the basis of its ESI mass spectra. The remarkable stability of **2** has allowed us to study some aspects of its biologically relevant reactivity, which are detailed below.

**Oxygen-atom exchange with water:** Because of the biological relevance of water exchange reactions at metal centers,<sup>[57]</sup> the ability of **2** to exchange its oxo ligand with  $\text{H}_2^{18}\text{O}$  was studied by taking advantage of ESI-MS. Complex **2** was generated by reaction of **1** with two equivalents of  $\text{CH}_3\text{CO}_3\text{H}$  in acetonitrile. Subsequently, 600 equivalents of  $\text{H}_2^{18}\text{O}$  were added to the reaction solution of **2**, and several ESI mass spectra were taken over time. The initial single peak at  $m/z$  469.1 associated with  $[\{\text{Fe}^{\text{IV}}(\text{O})(\text{Me,H-Pytcn})\}(\text{CF}_3\text{SO}_3)]^+$  decreased gradually, while a new peak at  $m/z$  471.1 corresponding to  $[\{\text{Fe}^{\text{IV}}(\text{O})(\text{Me,H-Pytcn})\}(\text{CF}_3\text{SO}_3)]^+$  appeared. Exchange of the oxygen atom with labeled water was complete in approximately 3 min at room temperature. Addition of pyridine-*N*-oxide, a strong  $\sigma$ -donating ligand, inhibited the water exchange exhibited by **2**, which suggested that the available coordination site in a *cis* configuration with respect to the oxo group plays an important role in facilitating the water exchange process.

Kinetic analyses of water exchange in **2** were performed by monitoring  $^{18}\text{O}$  incorporation into **2** directly by ESI-MS, and indirectly by quenching of a solution of **2** and  $\text{H}_2^{18}\text{O}$

with thioanisole at different reaction times and analyzing by GC-MS the percentage of labeled sulfoxide generated. Within experimental error, the two methods afforded identical reaction rates, thus supporting the validity of the second approach. In any case, exchange rate constants were obtained by nonlinear regression fitting of the data to a single exponential function.

The rate of water incorporation into **2** ( $k_{\text{obs}}$ ) was found to be linearly dependent on  $[\text{H}_2^{18}\text{O}]$  and independent of  $[\mathbf{2}]$ . The data are consistent with the rate law in Equation (1), in which the use of a relatively large  $[\text{H}_2^{18}\text{O}]$  allows for its analysis as a pseudo-first-order reaction [Eq. (1)]:

$$\frac{d[\text{Fe}^{\text{IV}}=^{18}\text{O}]}{dt} = k_{\text{exc}}[\text{Fe}^{\text{IV}}=^{16}\text{O}][\text{H}_2^{18}\text{O}] = k_{\text{obs}}[\text{Fe}^{\text{IV}}=^{16}\text{O}] \quad (1)$$

A bimolecular rate constant of  $k_{\text{exc}} = (0.028 \pm 0.003) \text{M}^{-1} \text{s}^{-1}$  at 295 K was extracted from this analysis. Activation parameters for water exchange were also determined by measuring exchange rates between 275 and 305 K, which afforded  $\Delta H^\ddagger = (10.2 \pm 0.8) \text{kcal mol}^{-1}$  and  $\Delta S^\ddagger = (-32 \pm 3) \text{cal K}^{-1} \text{mol}^{-1}$  (Figure 6). The negative activation entropy

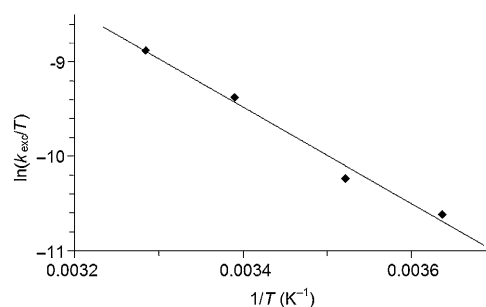


Figure 6. Eyring plot for the determination of the activation parameters of the oxygen-atom exchange of **2** with  $\text{H}_2^{18}\text{O}$  ( $[\text{H}_2^{18}\text{O}] = 0.2 \text{M}$ ).

is consistent with an associative event in the transition state, most likely a bimolecular collision between the  $\text{Fe}^{\text{IV}}(\text{O})$  species and a water molecule. Second-order rate constants for water exchange at  $[\text{Fe}^{\text{IV}}(\text{O})(\text{tpa})(\text{S})]^{2+}$  were also measured (Table 1). The accumulated data indicate that the water exchange rate for **2** is substantially faster than those for  $[\text{Fe}^{\text{IV}}(\text{O})(\text{tmc})(\text{CH}_3\text{CN})]^{2+}$  and  $[\text{Fe}^{\text{IV}}(\text{O})(\text{N4Py})]^{2+}$ , which lack *cis*-available sites to the oxo ligand, and also somewhat faster than that of  $[\text{Fe}^{\text{IV}}(\text{O})(\text{tpa})(\text{S})]^{2+}$ . Nevertheless, considering the pentadentate nature of N4Py, the higher reaction rate observed for **2** represents a rather modest enhancement. Furthermore, the smaller reaction rate measured for  $[\text{Fe}^{\text{IV}}(\text{O})(\text{tpa})(\text{S})]^{2+}$  suggests that reaction rates are not solely determined by the presence of a *cis*-labile site. Analysis of the enthalpy and entropy activation parameters indicates that the faster exchange rate in **2** has an entropic origin, which compensates for its higher activation enthalpy.

Table 1. Kinetic parameters for the water exchange reaction at selected oxo-iron(IV) complexes.

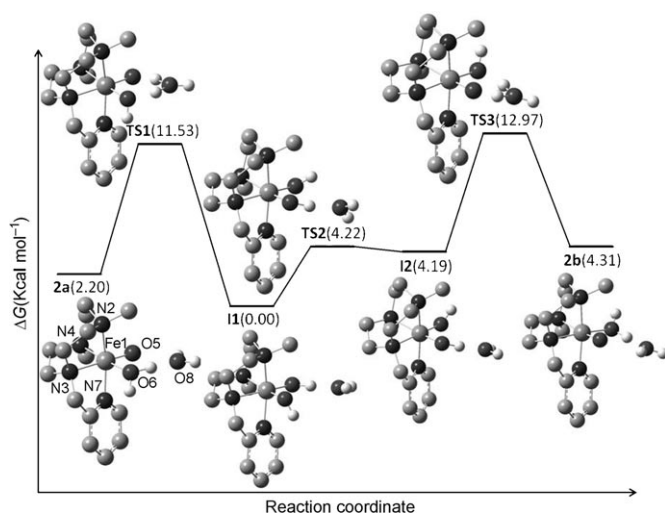
Compound	$k_{\text{exc}} \times 10^{-3}$ [M <sup>-1</sup> s <sup>-1</sup> ] <sup>[a]</sup>	$\Delta H^\ddagger$ [kcal mol <sup>-1</sup> ]	$\Delta S^\ddagger$ [cal K <sup>-1</sup> mol <sup>-1</sup> ]	Ref.
<b>2</b>	28 ± 3	10.2 ± 0.8	-32 ± 3	-
[Fe(O)(tmc)(CH <sub>3</sub> CN)] <sup>2+</sup>	2.0 <sup>[b]</sup>	4.1 ± 0.6	-57 ± 8	[44]
[Fe(O)(N4Py)] <sup>2+</sup>	2.4 <sup>[b]</sup>	4.0 ± 0.6	-57 ± 8	[44]
[Fe(O)(tpa)(S)] <sup>2+</sup>	8 ± 2	<sup>[c]</sup>	<sup>[c]</sup>	-

[a] At 295 K. [b] Calculated from experimental data in ref. [44]. [c] Eyring analysis could not be performed because of limited thermal stability.

### Computational analysis of the water exchange mechanism:

An obvious goal arising from these studies is to establish the fundamental chemical steps by which **2** can exchange its oxygen atom with water. The answers to this question may be of fundamental interest due to the structural similarity between **2** and biologically relevant non-heme oxo-iron(IV) species, in which the oxo group binds in a *cis* configuration with respect to one or more available coordination sites. In the heme paradigm, the incorporation of oxygen from water is explained by the so-called oxo-hydroxo tautomerism proposed by Meunier and Bernadou,<sup>[41]</sup> which entails the binding of labeled water *trans* to the oxo group and then tautomerization of this species to a symmetric *trans*-dihydroxo-iron(IV) intermediate that scrambles the label (Scheme 1). This pathway clearly cannot be operative for **2**, since there is no binding site *trans* to the oxo group available for coordination with water, and an alternative mechanism must apply in the present case. The mechanism depicted in Figure 7 starts with the iron(IV)-oxo complex **2a**, with a coordinated water molecule in a *cis* position with respect to the oxo group. In the DFT study<sup>[49,58]</sup> of the water exchange mechanism, the solvent effects and the dispersion correction have been taken into account in the single-point calculations. Solvent effects for acetonitrile were computed using the polarizable continuum model (PCM)<sup>[59]</sup> as implemented in Gaus-

sian 09.<sup>[50]</sup> The dispersion energy has been computed using the DFT-D3 method and program of Grimme et al.<sup>[60]</sup> According to our theoretical calculations,<sup>[58]</sup> a key aspect of the reaction is the presence of an exogenous water molecule at close distance to the oxo group and the water ligands. In the first step the exogenous water assists the transfer of one H<sup>+</sup> ion from the bound H<sub>2</sub>O to the oxo ligand, via a transition state (**TS1**), with a barrier of  $\Delta G^\ddagger = 9.3$  kcal mol<sup>-1</sup>. After the first proton-transfer event, an Fe<sup>IV</sup>(OH)<sub>2</sub> species (intermediate **I1**) is formed which is energetically favored compared to the starting complex **2a** by 2.2 kcal mol<sup>-1</sup>. Our spectroscopic data do not provide evidence for a significant accumulation of **I1** in solution, but a dihydroxomanganese(IV) species has recently been described for a related macrocyclic N<sub>4</sub> ligand,<sup>[61]</sup> and analogous LFe<sup>IV</sup>(OH)<sub>2</sub> species have been proposed on the basis of DFT methods for a bispidine-based complex (Scheme 2).<sup>[32,62]</sup> It is possible that the energy of **I1** is underestimated in our calculations, and that it is slightly higher in energy than the corresponding oxo-aqua isomeric species (see also below for a discussion based on computed Mössbauer parameters). In **I1**, the exogenous water molecule has a H-bond interaction with the O5H hydroxide ligand (oxo group in **2a**). In the next step, the exogenous water changes its interaction from the O5H hydroxo group to the second hydroxo ligand (O6H, aqua in **2a**) and the intermediate **I2** is formed. This step is endothermic with a free energy cost of 4.2 kcal mol<sup>-1</sup>. When the free energy corrections are included, **TS2** and **I2** are essentially isoenergetic. Close inspection reveals that **TS2** and **I2** differ in the orientation of the O5-H bond, which is not involved in hydrogen bonding with the external water molecule. **I2** evolves through a second H<sup>+</sup> transfer, passing through **TS3** and forming **2b**, in which the oxo ligand is *cis* to the NCH<sub>2</sub>py ligand. Considering that **TS2** and **I2** are nearly isoenergetic, the larger barrier along the overall process is **TS2+TS3** with  $\Delta G^\ddagger = 13.0$  kcal mol<sup>-1</sup>, and corresponds to the second proton transfer. Proton transfer not assisted by the second water molecule has an activation enthalpy barrier about three times higher. Isomer **2b** could not be experimentally observed because it is 2.11 kcal mol<sup>-1</sup> higher in energy than **2a**, and because the activation barriers associated with each of the elemental steps that connect the backwards conversion of **2a** to **2b** are small. In this scenario, water ligand exchange at **2b** and microscopic microreversibility lead to the formation of **2a**, in which the oxygen atom of the oxo group (*trans* to a NCH<sub>2</sub>py unit) comes from water. Interestingly, the mechanism for water exchange at **2** bears resemblance to the DFT-computed conversion of [Fe<sup>IV</sup>(OH)<sub>2</sub>L]<sup>2+</sup> (in which L is a tetradentate bispidine ligand related to bpd, Scheme 2) to [Fe<sup>IV</sup>(O)(OH)<sub>2</sub>L]<sup>2+</sup>.<sup>[32,62]</sup> Calculations indicate that this formal tautomerization takes place with a small energy barrier of 8.3 kcal mol<sup>-1</sup>. Unlike in **2**, the reaction involves a spin crossover from the *S* = 1 Fe<sup>IV</sup>(OH)<sub>2</sub> to the thermodynamically more stable ( $4.4$  kcal mol<sup>-1</sup>) *S* = 2 Fe<sup>IV</sup>(O)(OH)<sub>2</sub> tautomer, without the assistance of a second water molecule. In contrast, all iron(IV) species in our calculations remain on the *S* = 1 surface.

Figure 7. DFT mechanism for water exchange at **2**.

Taking this computed mechanism into consideration, the first-order kinetic dependence on water concentration is attributed to the initial equilibrium step involving the binding of a labeled water molecule, which replaces the initially bound unlabeled water. Nam, Que, and co-workers have proposed that a seven-coordinate *cis*-oxo-aqua intermediate is formed in the first step of the reaction between  $[\text{Fe}(\text{O})(\text{N4Py})]^{2+}$  and  $[\text{Fe}(\text{O})(\text{tmc})(\text{CH}_3\text{CN})]^{2+}$  with water (Scheme 1).<sup>[34]</sup> Such a mechanism may also be possible for **2** and  $[\text{Fe}(\text{O})(\text{tpa})(\text{S})]^{2+}$ , but owing to the presence of the labile water/acetonitrile ligand, a six-coordinate intermediate **2b** formed via a ligand-exchange reaction is favored. The breaking of the Fe–OH<sub>2</sub> bond is likely to be the origin of the higher activation enthalpy which, however, is entropically compensated because of the dissociative nature of the event.

An obvious consequence of the present mechanism is that, owing to the asymmetry of the two *cis*-labile sites, oxygen incorporation from water into the oxo ligand requires two oxo–hydroxo tautomerism reactions. That constitutes a fundamental mechanistic difference from oxygen-atom incorporation from water in metalloporphyrins.<sup>[41]</sup>

**DFT computation of the Mössbauer parameters of the species implicated in the water exchange mechanism:** Considering that the DFT-computed water exchange mechanism predicts that tautomeric bis-hydroxo-iron(IV) (**11** and **12**) and oxo-iron(IV) (**2a** and **2b**) are close in energy, the corresponding Mössbauer parameters were calculated with DFT methods and the results are collected in Table 2 (see the Ex-

Table 2. DFT-calculated Mössbauer parameters<sup>[a]</sup> of oxo-iron(IV) (**2a** and **2b**) and bis-hydroxo-iron(IV) (**11** and **12**) tautomeric species.

Compound	$\Delta E_{\text{O}}$ [ $\text{mm s}^{-1}$ ] <sup>[a]</sup>	$\delta$ [ $\text{mm s}^{-1}$ ]
<b>2a</b>	0.57	0.18
<b>11</b>	2.28	0.12
<b>12</b>	2.44	0.18
<b>2b</b>	0.83	0.17
Exp.	0.73	0.05

[a] See experimental section for details of the DFT analysis.

perimental Section for details of the DFT analysis). The calculated isomer shifts for **2a** and **2b** are a bit too high relative to the experimental values. The Pittsburgh group, using Gaussian with the B3LYP functional (calibration of Vrajmasu et al.<sup>[14a]</sup>), observed that the calculated  $\delta$  values for tmc come out quite well whereas those of most Fe<sup>IV</sup>=O complexes with pyridine and amine ligands are generally too high, by as much as 0.09  $\text{mm s}^{-1}$ . For the question at hand it is significant that the  $\Delta E_{\text{O}}$  values of **11** and **12** are much larger than those of **2a** and **2b**. In agreement, large  $\Delta E_{\text{O}}$  values have been reported for  $[\text{Fe}^{\text{IV}}(\text{OH})(\text{OO}t\text{Bu})(\text{bpmcn})]^{2+}$ <sup>[14b]</sup> ( $\Delta E_{\text{O}} = 1.75 \text{ mm s}^{-1}$ ) and the Fe<sup>IV</sup>-OH site of  $[(\text{OH})(\text{L}_{\text{OMe}})\text{Fe}^{\text{IV}}(\mu\text{-O})\text{Fe}^{\text{IV}}(\text{O})(\text{L}_{\text{OMe}})]^{3+}$  ( $\text{L}_{\text{OMe}} = \text{tris}[(4\text{-methoxy-3,5-dimethylpyridin-2-yl})d_2\text{-methyl}]\text{amine}$ ,  $\Delta E_{\text{O}} = 1.96 \text{ mm s}^{-1}$ ).<sup>[14c]</sup> We conclude that, despite **11** being the

lower-energy species in the DFT-calculated mechanism, the Mössbauer parameters favor the oxo-iron(IV) formulation, in agreement with the resonance Raman evidence for an Fe=O unit.

**Oxidation of sulfides: oxygen-atom transfer:** The oxygen-atom transfer ability of **2** was evaluated for the oxidation of sulfides. Complex **2** reacted rapidly at 273 K in CH<sub>3</sub>CN with 10 equivalents of thioanisole affording the corresponding sulfoxide (methylphenyl sulfoxide) in 98% yield. The reaction was monitored with UV/Vis spectroscopy by following the decrease of the band at 750 nm characteristic of the iron(IV)-oxo complex **2**. Under conditions of excess substrate (5–50 equiv with respect to **2**), the reactions showed pseudo-first-order behavior so that the observed reaction rates ( $k_{\text{obs}}$ ) were linearly dependent on substrate concentration. From this analysis, a second-order rate constant ( $k_{\text{H}}$ ) of  $(1.0 \pm 0.1) \text{ M}^{-1} \text{ s}^{-1}$  was obtained for the oxidation of thioanisole (see the Supporting Information). Additional information about the mechanism of this transformation was gained through the initial observation that the reaction rates were highly dependent on the *para* substituent of the aromatic ring. Thus, we measured the second-order rate constants ( $k_{\text{X}}$ ) for a series of *para*-substituted methyl phenyl sulfides, *p*-X-thioanisoles (X = CN, Cl, CH<sub>3</sub>, OCH<sub>3</sub>). Plotting of  $\log(k_{\text{X}}/k_{\text{H}})$  for the different substrates against the corresponding Hammett parameters ( $\sigma_{\text{p}}$ ) afforded a good linear correlation, and a Hammett value of  $\rho = -1.5$  was obtained (Figure 8). The negative  $\rho$  value reflects the electrophilicity

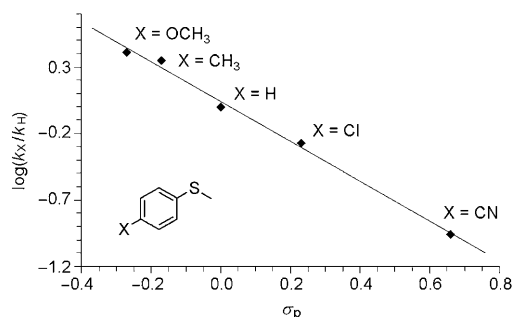


Figure 8. Hammett plot representing  $\log(k_{\text{X}}/k_{\text{H}})$  against the Hammett parameter ( $\sigma_{\text{p}}$ ) for the reaction of **2** with *p*-X-thioanisoles at 273 K.

of the oxo group in **2**. On the other hand, a plot of  $\log(k_{\text{X}})$  against the one-electron oxidation potentials of each *p*-X-thioanisole ( $E^{\circ}_{\text{ox}}$ ) afforded a linear correlation with a slope of  $-3.0$  (see the Supporting Information). As slope values around 10 would have been expected for a process initiated by one-electron transfer,<sup>[63,64]</sup> the observed slope of 3 indicates that the oxidation of sulfides by **2** does not occur by such a process but rather through a direct oxygen-atom transfer mechanism. Further evidence for a direct oxygen-atom transfer between the terminal oxo ligand and the sulfide came from labeling of the oxo group with <sup>18</sup>O. This was achieved by oxygen-atom exchange of **2** with H<sub>2</sub><sup>18</sup>O and sub-

sequent reaction of the resulting  $[\text{Fe}^{\text{IV}}(^{18}\text{O})(^{\text{Me,H}}\text{Pytacn})(\text{H}_2\text{O})]^{2+}$  with thioanisole. Analysis of the resulting sulfoxide by GC-MS indicated that 80% of the product was labeled with  $^{18}\text{O}$ .

Despite the similarities between the oxygen-atom transfer process in **2** and in other synthetically prepared iron(IV)-oxo species, reaction rates are highly dependent on the specific structure of the ligand. In particular, the oxidation of thioanisole by  $[\text{Fe}^{\text{IV}}(\text{O})(\text{N4Py})]^{2+}$  and  $[\text{Fe}^{\text{IV}}(\text{O})(\text{Bn-tpen})]^{2+}$  (Scheme 2) afforded second-order rate constants of 0.065 (273 K) and  $0.075 \text{ M}^{-1} \text{ s}^{-1}$  (253 K), respectively, and this rate was even smaller for  $[\text{Fe}^{\text{IV}}(\text{O})(\text{tmc})(\text{CH}_3\text{CN})]^{2+}$  for which a value of  $0.029 \text{ M}^{-1} \text{ s}^{-1}$  at 35 °C was obtained.<sup>[31]</sup> Comparison with the reactivity of  $[\text{Fe}^{\text{IV}}(\text{O})(\text{tpa})(\text{S})]^{2+}$  is hampered due to its inherent instability, which prevents proper measurement of the second-order rate constant at relatively high temperatures (a value of  $0.44 \text{ M}^{-1} \text{ s}^{-1}$  corresponding to the reaction with thioanisole at 228 K has been reported).<sup>[31]</sup> Nevertheless, from these studies it can be concluded that **2** and  $[\text{Fe}^{\text{IV}}(\text{O})(\text{tpa})(\text{S})]^{2+}$ , both of which bear tripodal tetradentate-based ligands, are much more reactive in the oxygen-atom transfer reaction than the corresponding complexes bearing tmc (tetradentate planar) or N4Py and Bn-tpen (pentadentate) ligands.

**Oxidation of activated C–H bonds: hydrogen-atom abstraction:** The reactions of **2** with a series of substrates for H-atom abstraction were studied. Complex **2** reacted with 5 equivalents of 9,10-dihydroanthracene (DHA) at 258 K affording anthracene as the only product detected by GC-MS. When the reaction was run under  $\text{N}_2$ , 0.45 mmol anthracene per mmol of **2** was measured. The UV/Vis spectra at the end of the reactions did not show formation of **1**. In addition, the ESI mass spectrum of the resulting solution was dominated by ions corresponding to mononuclear  $\text{Fe}^{\text{III}}$  species. Therefore, considering that Mössbauer spectra indicate a 85(5)%  $\text{Fe}^{\text{IV}}$  content in our preparations, on the basis of stoichiometric considerations we conclude that in this reaction **2** acts as a  $1e^-$  oxidant (Scheme 4), and that the yield of the reaction with DHA is nearly quantitative.



Scheme 4.

The kinetics of reactions of **2** with a series of substrates were studied by UV/Vis spectroscopy following the decay of the band at 750 nm characteristic of the iron(IV)-oxo species **2**. The decay of **2** followed good first-order kinetics under conditions of excess substrate and  $k_{\text{obs}}$  values were linearly dependent on substrate concentration in all cases, thus allowing us to determine the corresponding second-order rate constants,  $k_2$  (see the Supporting Information). These values are collected in Table 3. Reaction of **2** with alkylaromatic substrates (toluene and ethylbenzene) caused rapid

Table 3. C–H bond dissociation energies (BDEs) and rates for the reaction of **2** with different substrates.<sup>[a]</sup>

Substrate	BDE [kcal mol <sup>-1</sup> ] <sup>[67,68]</sup>	$k_2$ [M <sup>-1</sup> s <sup>-1</sup> ]
10-methyl-9,10-dihydroacridine (AcrH <sub>2</sub> )	73.7	86 ± 19
xanthene	75.5	8.1 ± 0.8
9,10-dihydroanthracene (DHA)	77	5.7 ± 0.9
1,4-cyclohexadiene (CHD)	78	4.2 ± 0.3
fluorene	80	1.2 ± 0.2
2,3-dimethyl-2-butene	84	$(1.6 \pm 0.2) \times 10^{-2}$
tetrahydrofuran (THF)	93	$(2.3 \pm 0.3) \times 10^{-3}$
cyclohexane <sup>[b]</sup>	99.3	$(4 \pm 1) \times 10^{-4}$

[a] Reactions were run in acetonitrile at 258 K, with **2** generated in situ from the reaction of **1** (1 mM) with 2 equiv peracetic acid at 15 °C. [b] 298 K.

formation of brown–dark blue intense chromophores, indicative of alkylphenolate-bound iron(III) species. Considering the high bond dissociation energy (BDE) of the C–H bond in aromatic substrates, such reactions could not occur through H-atom abstraction but instead they originate from electrophilic attack of the aromatic ring by **2**.<sup>[37]</sup> For this reason, these substrates were not further addressed in the present study.

Complex **2** proved to be a very powerful oxidant in C–H oxidation reactions (Tables 3 and 4). Compared to related dicationic iron(IV)-oxo complexes under analogous condi-

Table 4. DHA oxidation rates of various iron-oxo complexes.<sup>[a]</sup>

Complex	$k_2$ [M <sup>-1</sup> s <sup>-1</sup> ]	T [K]	Ref.
<b>2</b>	5.7 ± 0.9	258	
$[\text{Fe}^{\text{IV}}(\text{O})(\text{N4Py})]^{2+}$	2.8	258	[75]
$[\text{Fe}^{\text{IV}}(\text{O})(\text{bpd})(\text{CH}_3\text{CN})]^{2+}$	8.0	238	[35]
$[\text{Fe}^{\text{IV}}(\text{O})(\text{tmc})(\text{CH}_3\text{CN})]^{2+}$	0.016	243	[24]
$[\text{Fe}^{\text{III}}(\text{OMe})(\text{Py5})]^{2+}$	$5.0 \times 10^{-3}$	298	[66]
$[(\text{OH})(\text{L}_{\text{OMe}})\text{Fe}^{\text{III}}(\mu\text{-O})\text{Fe}^{\text{IV}}(\text{O})(\text{L}_{\text{OMe}})]^{2+}$	28	193	[65]
$[\text{Fe}^{\text{III}}\text{Fe}^{\text{IV}}(\mu\text{-O})_2(\text{L}_{\text{OMe}})_2]^{3+}$	$10^{-5}$	193	[65]
$[\text{Fe}^{\text{IV}}_2(\mu\text{-O})_2(\text{L}_{\text{OMe}})_2]^{4+}$	$10^{-4}$	193	[65]
$[(\text{OH})(\text{L}_{\text{OMe}})\text{Fe}^{\text{IV}}(\mu\text{-O})\text{Fe}^{\text{IV}}(\text{O})(\text{L}_{\text{OMe}})]^{3+}$	0.027	193	[65]
$[\text{Fe}^{\text{IV}}(\text{O})(\text{tmp})]$	2.7	258	[76]
$[\text{Fe}^{\text{IV}}(\text{O})(\text{TMG}_3\text{tren})]^{2+}$	0.090	243	[24]

[a]  $\text{L}_{\text{OMe}}$  = tris[(4-methoxy-3,5-dimethylpyridin-2-yl)*d*<sub>2</sub>-methyl]amine, tmp = tetramesitylporphinate,  $\text{TMG}_3\text{tren}$  = 1,1,1-tris[2-[N<sup>2</sup>-(1,1,3,3-tetramethylguanidino)]ethyl]amine.

tions, reaction rates obtained with **2** are somewhat higher than those obtained with  $[\text{Fe}^{\text{IV}}(\text{O})(\text{N4Py})]^{2+}$  and nearly two orders of magnitude faster than with  $[\text{Fe}^{\text{IV}}(\text{O})(\text{tmc})(\text{CH}_3\text{CN})]^{2+}$ <sup>[24,34]</sup> but somewhat lower than that found for  $[\text{Fe}^{\text{IV}}(\text{O})(\text{bpd})(\text{CH}_3\text{CN})]^{2+}$  (Scheme 2).<sup>[35]</sup> Furthermore, the second-order rate constant for the oxidation of DHA with **2** appears to be several orders of magnitude higher than those reported for low-spin  $\text{Fe}^{\text{III}}\text{Fe}^{\text{IV}}$  and  $\text{Fe}^{\text{IV}}\text{Fe}^{\text{IV}}$  oxo-dimers, and approaches the remarkably high rate ( $k_2 = 28 \text{ M}^{-1} \text{ s}^{-1}$  at 193 K) recently measured for the high-spin  $[(\text{HO})(\text{L}_{\text{OMe}})\text{Fe}^{\text{III}}\text{-O-Fe}^{\text{IV}}(\text{O})(\text{L}_{\text{OMe}})]^{2+}$ , in which  $\text{L}_{\text{OMe}}$  = tris[(4-methoxy-3,5-dimethyl-pyridin-2-yl)methyl]amine (Table 4).<sup>[65]</sup> The high reactivity of the latter has been rationalized on the

basis of the high spin ( $S=2$ ) state of the iron ions, and the compound has limited stability even at  $-80^{\circ}\text{C}$ . On the other hand, as already discussed, the metal ion found in **2** has an  $S=1$  spin state, and it is moderately stable at room temperature. As expected from its higher oxidation state, reaction rates with **2** are 2–3 orders of magnitude faster than those obtained with the lipoxygenase model  $[\text{Fe}^{\text{III}}(\text{OMe})(\text{Py}5)]^{2+}$  ( $\text{Py}5=2,6\text{-bis}[\text{bis}(2\text{-pyridyl})\text{methoxymethane}]\text{pyridine}$ ).<sup>[66]</sup> Indeed, **2** proved to be competent for performing the oxidation of strong C–H bonds such as those in THF ( $\text{BDE}=93\text{ kcal mol}^{-1}$ ) with a reaction rate  $k_2=(2.3\pm 0.3)\times 10^{-3}\text{ M}^{-1}\text{ s}^{-1}$  at 258 K.<sup>[67]</sup> Most remarkably, **2** is also competent to perform the oxidation of cyclohexane ( $\text{BDE}=99.3\text{ kcal mol}^{-1}$ ) at room temperature with a second-order rate constant, after correction for the number of C–H bonds, of  $k'_2=3.6\times 10^{-5}\text{ M}^{-1}\text{ s}^{-1}$ . GC analysis of the reactions revealed the formation of 0.12 mol cyclohexanone per mol of **2** and 0.28 mol cyclohexanol per mol of **2**. Nevertheless, this reaction rate is relatively slow when compared with the fast oxidation observed in catalytic  $1/\text{H}_2\text{O}_2$  cyclohexane oxidations, in which an  $[\text{Fe}^{\text{V}}(\text{O})(\text{OH})(\text{Me}_6\text{H}^{\text{P}}\text{Pytacn})]^{2+}$  species has been inferred from isotopic labeling experiments and DFT analysis.<sup>[45,50]</sup>

Comparative reactivity profiles of the reactions of **2** against different substrates show that the rate constants decreased with the increase of the C–H BDE and more interestingly the  $\log(k'_2)$  values correlated linearly with the C–H BDE values of the substrates, giving a slope of approximately  $-0.2$  (Table 3, Figure 9). The slope is comparable to those

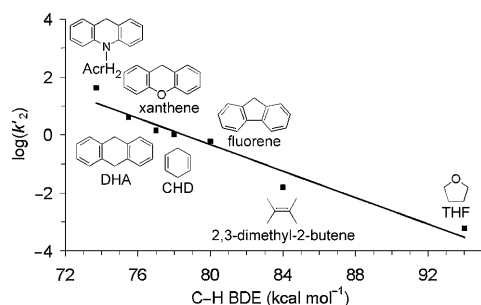


Figure 9. Plot of  $\log(k'_2)$  (determined at  $-15^{\circ}\text{C}$ ) against the C–H BDE of different substrates.

obtained for hydrogen abstraction reactions mediated by  $[\text{Fe}^{\text{IV}}(\text{O})(\text{N}4\text{Py})]^{2+}$ <sup>[16]</sup> and  $[\text{Fe}^{\text{III}}(\text{OMe})(\text{Py}5)]^{2+}$ ,<sup>[66]</sup> and intermediate between the  $-0.4$  and  $-0.1$  observed for  $[\text{Ru}^{\text{IV}}(\text{O})(\text{bpy})_2(\text{py})]^{2+}$  and  $[\text{Mn}^{\text{III}}(\text{OMe})(\text{Py}5)]^{2+}$ ,<sup>[69,70]</sup> respectively. Such a correlation strongly suggests that reactions take place through a H-atom abstraction mechanism,<sup>[69,71–73]</sup> as earlier established for related  $\text{Fe}^{\text{IV}}$  compounds.<sup>[18,34,74]</sup>

Parallel reactions with deuterated DHA ( $d_4\text{-DHA}$ ) yielded a kinetic isotope effect (KIE) of 27, a value which is consistent with C–H bond cleavage being the rate-determining step.<sup>[68]</sup> This large KIE value is well above the semiclassical limit of 7, thus suggesting a hydrogen-atom transfer mecha-

nism dominated by quantum mechanical tunneling.<sup>[74,77,78]</sup> For comparison, KIE values around 17 were obtained for the oxidation of DHA by  $[\text{Fe}^{\text{IV}}(\text{O})(\text{tmc})(\text{X})]^{2+}$  ( $\text{X}=\text{CH}_3\text{CN}$ ,  $\text{CF}_3\text{COO}^-$ , or  $\text{N}_3^-$ )<sup>[34]</sup> and even larger values were reported in the oxidation of benzyl alcohol by  $[\text{Fe}^{\text{IV}}(\text{O})(\text{N}4\text{Py})]^{2+}$  (KIE = 48) and  $[\text{Fe}^{\text{IV}}(\text{O})(\text{tpa})(\text{S})]^{2+}$  (KIE = 58).<sup>[33]</sup> Moreover, such large isotope effects have also been observed in hydrogen-atom abstraction reactions performed by the iron(IV)-oxo intermediate of TauD (KIE  $\approx 37$ ),<sup>[79]</sup> the iron(III)-hydroxo active species of lipoxygenase (KIE  $\approx 50$ ),<sup>[80]</sup> and compound Q ( $\text{Fe}^{\text{IV}}\text{Fe}^{\text{IV}}$ ) of the diiron enzyme soluble methane monooxygenase (sMMO) (KIE > 50).<sup>[81]</sup>

A particular case that deserves some comment is the reaction with the nicotinamide adenine dinucleotide (NADH) analogue 10-methyl-9,10-dihydroacridine ( $\text{AcrH}_2$ ), which is considered a hydride donor.<sup>[82]</sup> The reaction of  $\text{AcrH}_2$  with **2** results in rapid formation ( $k_2=(86\pm 19)\text{ M}^{-1}\text{ s}^{-1}$ ) of the acridinium cation  $\text{AcrH}^+$ , as evidenced by UV/Vis spectroscopy. UV/Vis quantification based on the characteristic spectral features of the cation accounts for 1 mmol  $\text{AcrH}^+$  per mmol **2**, which indicates that **2** acts as a  $2e^-$  oxidant and that the reaction is best described as a formal hydride transfer to the iron(IV)-oxo moiety. Interestingly, the corresponding oxidation rate constant ( $k'_2$ ) appears to be only slightly faster than expected from the  $\log(k'_2)$  versus BDE graph correlation (Figure 9), thus suggesting that a common rate-determining step is operative for all the series of substrates plotted. In addition, the KIE value obtained from the reaction of **2** with  $\text{AcrD}_2$  at 258 K is 4.7 (Figure S11 in the Supporting Information), which is intermediate between the values observed for  $[\text{Fe}^{\text{IV}}(\text{O})(\text{N}4\text{Py})]^{2+}$  (KIE = 13.5)<sup>[82]</sup> and those obtained recently with  $[\text{Fe}^{\text{IV}}(\text{O})(\text{bpd})(\text{CH}_3\text{CN})]^{2+}$  (KIE = 2.3; Scheme 2).<sup>[35]</sup> On this basis, we propose that the reaction takes place through a rate-determining hydrogen-atom abstraction that can be regarded as a proton-coupled electron transfer, followed by a fast electron transfer.<sup>[68,76,83,84]</sup>

Considering that C–H bond oxidation by **2** occurs through a hydrogen-atom abstraction mechanism,<sup>[73,85,86]</sup> the balance between the strength of the cleaved C–H bond and of the formed  $\text{Fe}^{\text{III}}\text{–OH}$  bond must determine the observed reaction rates. Along this interpretation, we notice that reactions mediated by **2** are comparable to those associated with the most reactive  $\text{Fe}^{\text{IV}}(\text{O})$  species containing nitrogen-based pentadentate ligands such as  $[\text{Fe}^{\text{IV}}(\text{O})(\text{N}4\text{Py})]^{2+}$ , which constitute one of the very rare examples of well-defined metal-oxo species that are capable of breaking the strong C–H bond of cyclohexane at room temperature.<sup>[18,87–89]</sup> The similar reaction rates observed for **2** and  $[\text{Fe}^{\text{IV}}(\text{O})(\text{N}4\text{Py})]^{2+}$  should be interpreted as both of them forming a  $\text{Fe}^{\text{III}}\text{O–H}$  bond of approximately the same energy. Previous literature reports on the estimation of the  $\text{Fe}^{\text{III}}\text{O–H}$  bond in  $[\text{Fe}^{\text{IV}}(\text{O})(\text{N}4\text{Py})]^{2+}$  have provided somewhat different values. Two independent theoretical studies yielded  $\text{Fe}^{\text{III}}\text{O–H}$  BDEs of 84<sup>[90,91]</sup> and 97  $\text{kcal mol}^{-1}$ ,<sup>[92]</sup> and some of us have experimentally estimated a more modest  $\text{BDE}=78\text{ kcal mol}^{-1}$  from its experimentally observed redox potential in water.<sup>[75]</sup> We can take the latter value as a lower limit estimate of the corre-

sponding Fe<sup>III</sup>O–H bond formed by H abstraction in **2**. Thus, as previously noted for [Fe<sup>IV</sup>(O)(N4Py)]<sup>2+</sup>,<sup>[90]</sup> despite its rather surprising thermal stability, **2** is a very powerful oxidant. Besides the high oxidation state, one of the reasons at the origin of such a high reactivity is likely to be the positive charge of the [LFe<sup>IV</sup>(O)]<sup>2+</sup> unit when L is a neutral ligand (N4Py or <sup>Me,H</sup>Pytacn), which results in a very electrophilic oxidant.

The remarkably high oxidative reactivity exhibited by **2** both in O-atom transfer and in H abstraction reactions is unprecedented and deserves some comment. The factors that determine the reactivity of oxo-iron(IV) species have been the focus of intense debate. The accessibility of multiple spin states modulated by the nature of the ligand *trans* to the oxo group has been invoked to explain inverted tendencies in oxygen-atom transfer versus H abstraction reaction by a series of Fe<sup>IV</sup> compounds.<sup>[34]</sup> Basic anionic ligands X in a series of [Fe<sup>IV</sup>(O)(X)(tmc)]<sup>+</sup> complexes decrease their electrophilicity and O-atom transfer reactivity, but enhance their H abstraction reactivity by populating a reactive quintet state. Population of an excited, more highly reactive *S*=2 state has also been proposed to account for the exceptional ability of [Fe<sup>IV</sup>(O)(N4Py)]<sup>2+</sup> to cleave strong C–H bonds through a H-atom abstraction mechanism.<sup>[90]</sup> The nature of the ligands *cis* to the oxo group is considered to have a more modest effect on the oxidative reactivity.<sup>[93]</sup> Computational studies have thus suggested that high-spin *S*=2 Fe<sup>IV</sup>(O) species could be much more reactive than their corresponding low-spin *S*=1 analogues. However, the recent preparation and characterization of the first synthetic *S*=2 Fe<sup>IV</sup>(O) species raises some questions about this prediction, because it exhibits reactivity only comparable to that of [Fe<sup>IV</sup>(O)(N4Py)]<sup>2+</sup>.<sup>[24,25]</sup> Steric effects were invoked by the authors to account for these observations. Complex **2** contains an *S*=1 spin state, and DFT computations show that it is well separated in energy from the *S*=2 spin state (see Table S7 in the Supporting Information). Therefore, a two-state reactivity (TSR) scenario appears highly unlikely. In addition, high reaction rates are measured for both O-atom transfer and H-atom abstraction reactions. Its high oxidative reactivity may then add to the rationale of substrate accessibility to the reactive oxo ligand as a major factor dictating reactivity in these species. The high reactivity of **2** in C–H oxidation reactions finds a nice precedent in that recently described for [Fe<sup>IV</sup>(O)(bpd)(CH<sub>3</sub>CN)]<sup>+2</sup> (Scheme 2).<sup>[35]</sup> Both compounds have a N<sub>4</sub>-based ligand that enforces a *cis*-oxo-labile site. However, the bispidine is a weaker-field ligand<sup>[32,62]</sup> than <sup>Me,H</sup>Pytacn,<sup>[50]</sup> and the TSR scenario is more likely. In this scenario, we propose that **2** is more reactive than most low-spin iron(IV)-oxo species bearing pentadentate and/or planar tetradentate ligands, because the oxo ligand in **2** is more exposed and susceptible to interaction with small substrate molecules. However, compared with previously reported tetradentate ligands, <sup>Me,H</sup>Pytacn affords a very significant degree of steric protection against bimetallic dimerization reactions.

## Conclusion

We have reported the preparation of a new *S*=1 iron(IV)-oxo species (**2**) with a tripodal tetradentate ligand that has remarkable thermal stability, especially when compared with structurally related complexes such as [Fe<sup>IV</sup>(O)-(bpmcn)(S)]<sup>2+</sup>, [Fe<sup>IV</sup>(O)(tpa)(S)]<sup>2+</sup>, and [Fe<sup>IV</sup>(O)(bpd)-(CH<sub>3</sub>CN)]<sup>+2</sup>. Complex **2** has a labile site *cis* to the oxo group, which constitutes a very common structural feature of non-heme iron oxygenases. Complex **2** rapidly exchanges its oxygen atom with H<sub>2</sub><sup>18</sup>O following a mechanism in which an exogenous water molecule assists the hydrogen transfer from the coordinated water molecule to the oxo group. Despite its remarkable thermal stability, **2** is a very good oxidant both with respect to oxygen-atom transfer to sulfides and hydrogen-atom abstraction of alkane C–H bonds, thus demonstrating a highly electrophilic character arising from the Fe<sup>IV</sup> oxidation state in a neutral N-based ligand environment. The higher oxidative reactivity of **2** when compared with complexes containing pentadentate ligands is attributed to the tetradentate nature of the <sup>Me,H</sup>Pytacn ligand, which does not provide steric encumbrance of the oxo ligand in **2**, thus providing the basis of its remarkable oxidative reactivity.

## Experimental Section

**Materials and methods:** Reagents and solvents used were of commercial available reagent quality unless otherwise stated. Preparation and handling of air-sensitive materials were performed under an inert atmosphere either on a Schlenk line or in a glove box. Acetonitrile was purchased from Scharlau. H<sub>2</sub><sup>18</sup>O (95% <sup>18</sup>O-enriched) was received from ICON Isotopes.

**Synthesis of complexes:** The starting complex [Fe(CF<sub>3</sub>SO<sub>3</sub>)<sub>2</sub>(<sup>Me,H</sup>Pytacn)] (**1**) was prepared by following the previously reported experimental procedure.<sup>[45]</sup> Preparation of iron(IV)-oxo complex **2** was performed as follows. Peracetic acid solution (2 equiv, 100 μL of a 40 mM solution in CH<sub>3</sub>CN obtained by dilution of commercially available 32% w/w peracetic acid solution in acetic acid) was added at 288 K to a solution of **1** in acetonitrile (1 mM, 2 mL total volume). The formation of **2** was followed by UV/Vis spectroscopy, which showed the appearance of a band at 750 nm ( $\lambda_{\text{max}}=200\text{ m}^{-1}\text{ cm}^{-1}$ ) with a shoulder at 900 nm that developed in about 10 min. The resulting solution of **2** (1 mM) was directly used for subsequent reactivity studies.

**Direct preparation of [Fe<sup>III</sup><sub>2</sub>(μ-O)(μ-CH<sub>3</sub>COO)(<sup>Me,H</sup>Pytacn)<sub>2</sub>-(ClO<sub>4</sub>)<sub>3</sub>·CH<sub>3</sub>CN (3·CH<sub>3</sub>CN):** Compound **1** (90 μmol, 54.6 mg) was dissolved in MeCN (2 mL) under an inert atmosphere. An acetonitrile solution (200 μL) 0.30 M in CH<sub>3</sub>COOH and Et<sub>3</sub>N (60 μmol CH<sub>3</sub>COOH and Et<sub>3</sub>N) were added at once, which caused an immediate color change from dark pink to bright yellow. Immediately a balloon filled with O<sub>2</sub> was connected to the reaction vessel and the solution became red-brown in a few seconds. After stirring for 3 h, the solvent from the resulting solution was removed under reduced pressure which afforded a brown oil. The resulting product was redissolved in acetonitrile and NaClO<sub>4</sub>·H<sub>2</sub>O (135 μmol, 19 mg) was added. The solution was stirred for about 2 h, filtered through Celite, and diethyl ether was slowly diffused. Brown crystals of **3**·CH<sub>3</sub>CN (37 mg) suitable for X-ray diffraction were obtained (38 μmol, 84%). <sup>1</sup>H NMR (200 MHz, CDCl<sub>3</sub>, 300 K): δ = 26.43, 18.27, 17.41, 14.47, 6.57 ppm; FTIR (ATR) ν = 1611, 1523 (CH<sub>3</sub>COO), 1447 (C=C<sub>ar</sub>), 1073, 621 cm<sup>-1</sup> (ClO<sub>4</sub>); UV/Vis (CH<sub>3</sub>CN): λ<sub>max</sub> (ε/Fe) = 427 (660),

462 (690), 513 (500), 692 nm ( $58 \text{ mol}^{-1} \text{ cm}^{-1}$ ); ESI-MS:  $m/z$ : 227.6 [ $M-3\text{ClO}_4$ ] $^{+3}$ , 880.9 [ $M-\text{ClO}_4$ ] $^{+}$ .

**Oxygen-atom exchange with water:** Kinetic studies on oxygen-atom exchange of **2** with  $\text{H}_2^{18}\text{O}$  were performed by quenching aliquots of the reaction mixture with thioanisole at different times, and analyzing by GC-MS the percentage of  $^{18}\text{O}$ -labeled methylphenyl sulfoxide generated. The pH dependence of the reaction rates was not studied. In a typical experiment, an appropriate amount of  $\text{H}_2^{18}\text{O}$  (6–60  $\mu\text{L}$ ) was added to a stirred solution of **2** in acetonitrile (2.5 mL, 1 mM) at once. At different reaction times, an aliquot of the reaction mixture (350  $\mu\text{L}$ ) was directly poured into a solution containing thioanisole (7  $\mu\text{L}$ ) in  $\text{CH}_3\text{CN}$  (300  $\mu\text{L}$ ). The resulting yellow solution was stirred for 30 min at room temperature, filtered through a short path of basic alumina, and washed with ethyl acetate (2 mL). The sample was analyzed by GC-MS. The percentage of  $^{18}\text{O}$ -labeled sulfoxide was determined by the isotopic pattern shown by the peaks at  $m/z$  125 and 140. In a typical experiment, a total of seven aliquots were removed from the reaction mixture. The temperature of the reaction mixture (0–30 °C) was controlled by means of a cryostat or a thermostated water bath. The percentage of  $^{18}\text{O}$ -labeled sulfoxide is directly related to the percentage of iron(IV)-oxo species **2** that has exchanged its oxygen atom with  $\text{H}_2^{18}\text{O}$ . The percentage of  $^{18}\text{O}$ -labeled sulfoxide over time could be fitted to a pseudo-first-order kinetics that allowed us to measure the rate constants ( $k_{\text{obs}}$ ) corresponding to oxygen-atom exchange with  $^{18}\text{O}$ -labeled water in **2**.

**Oxidation of activated C–H bonds and sulfides:** Appropriate amounts of substrates (diluted in acetonitrile) were added to a solution of **2** (1 mM) and the subsequent decay of the spectral changes corresponding to the iron(IV)-oxo species was directly monitored by UV/Vis spectroscopy. The kinetic studies were performed at specific temperatures: 273 K for the oxidation of sulfides and 258 K for the oxidation of activated C–H bonds. Unless specifically stated, reactions were carried out under air. Rate constants,  $k_{\text{obs}}$ , were determined by pseudo-first-order fitting of the decrease of the absorption band at 750 nm. Product analyses for the oxidation of thioanisole and DHA were performed by gas chromatography. Prior to injection, an internal standard (biphenyl) was added to the solution, which was further filtered through basic alumina and washed with ethyl acetate. Calibration curves with authentic products were generated to allow quantitative determination of the oxidized products.

**DFT calculations of the Mössbauer parameters:** Details of the DFT calculations are collected in the references. The  $\text{Fe}^{\text{IV}}$  DFT Mössbauer parameters were calculated at the OPBE/TZP<sup>[94]</sup> level within the conductor-like screening (COSMO) solvation model<sup>[95]</sup> (with dielectric constant  $\epsilon = 37.5$ , acetonitrile) by using the Amsterdam density functional (ADF) suite of programs.<sup>[96]</sup> The isomer shift ( $\delta$ ), which is proportional to the electron density [ $\rho(0)$ ] difference at the Fe nuclei between the studied system and a reference system (normaly  $\alpha\text{-Fe}$  at 300 K), was calculated according to the procedure described in ref. [97] with utility programs provided by Han and Noodleman. The isomer shift is given by [Eq. (2)]:

$$\delta = \alpha(\rho(0) - A) + C \quad (2)$$

in which  $\rho(0)$  is obtained by using the ADF and Han and Noodleman code,  $A$  is a constant chosen close to the electron density at the Fe nucleus in the reference state, and  $\alpha$  and  $C$  were determined by linear regression between the calculated  $\rho(0)$  and experimental  $\delta$  values. The Han and Noodleman code with their  $\text{Fe}^{2.5+}, 3+, 3.5+, 4+$  training set gave  $\alpha = (-0.312 \pm 0.022)$  and  $C = (0.373 \pm 0.014) \text{ mms}^{-1}$  for OPBE. The quadrupole splitting, which is proportional to the electric field gradient at the Fe nucleus, is directly given by the ADF.

## Acknowledgements

Financial support for this work was provided by MEC-Spain (Projects CTQ2009-08464/BQU and CTQ2008-06696/BQU), and the US National Institutes of Health (GM-33162 to L.Q. and EB-001475 to E.M.). M.C. acknowledges Generalitat de Catalunya for an ICREA-Academia Award and SGR 2009 SGR 637. A.C., I. P., and M.G. thank MEC for FPU PhD

grants. We thank RahuCat for a generous gift of tritosyl tacn. We thank W. Han and L. Noodleman for providing the utility programs to compute the Mössbauer parameters of the iron complexes and M. Swart for his useful comments about the Mössbauer calculations.

- [1] M. M. Abu-Omar, A. Loaiza, N. Hontzeas, *Chem. Rev.* **2005**, *105*, 2227.
- [2] M. Costas, M. P. Mehn, M. P. Jensen, L. Que, Jr., *Chem. Rev.* **2004**, *104*, 939.
- [3] E. I. Solomon, T. C. Brunold, M. I. Davis, J. N. Kemsley, S.-K. Lee, N. Lehnert, F. Neese, A. J. Skulan, Y.-S. Yang, J. Zhou, *Chem. Rev.* **2000**, *100*, 235.
- [4] J. M. Bollinger, Jr., J. C. Price, L. M. Hoffart, E. W. Barr, C. Krebs, *Eur. J. Inorg. Chem.* **2005**, 4245.
- [5] J. C. Price, E. W. Barr, B. Tirupati, J. M. Bollinger, Jr., C. Krebs, *Biochemistry* **2003**, *42*, 7497.
- [6] D. P. Galonic, E. W. Barr, C. T. Walsh, J. M. Bollinger, C. Krebs, *Nat. Chem. Biol.* **2007**, *3*, 113.
- [7] L. M. Hoffart, E. W. Barr, R. B. Guyer, J. J. M. Bollinger, C. Krebs, *Proc. Natl. Acad. Sci. USA* **2006**, *103*, 14738.
- [8] B. E. Eser, E. W. Barr, P. A. Frantom, L. Saleh, J. M. Bollinger, Jr., C. Krebs, P. F. Fitzpatrick, *J. Am. Chem. Soc.* **2007**, *129*, 11334.
- [9] M. L. Matthews, C. M. Krest, E. W. Barr, F. H. Vaillancourt, C. T. Walsh, M. T. Green, C. Krebs, J. M. Bollinger, Jr., *Biochemistry* **2009**, *48*, 4331.
- [10] O. Pestovsky, S. Stoian, E. L. Bominaar, X. Shan, E. Münck, L. Que, Jr., A. Bakac, *Angew. Chem.* **2005**, *117*, 7031–7034; *Angew. Chem. Int. Ed.* **2005**, *44*, 6871–6874.
- [11] J.-U. Rohde, J.-H. In, M.-H. Lim, W. W. Brennessel, M. R. Bukowski, A. Stubna, E. Münck, W. Nam, L. Que, Jr., *Science* **2003**, *299*, 1037.
- [12] K. Ray, J. England, A. T. Fiedler, M. Martinho, E. Münck, L. Que, Jr., *Angew. Chem.* **2008**, *120*, 8188; *Angew. Chem. Int. Ed.* **2008**, *47*, 8068.
- [13] M. H. Lim, J.-H. Rohde, A. Stubna, M. R. Bukowski, M. Costas, R. Y. N. Ho, E. Münck, W. Nam, L. Que, Jr., *Proc. Acad. Sci. USA* **2003**, *100*, 3665.
- [14] a) V. Vrajmasu, E. Münck, E. L. Bominaar, *Inorg. Chem.* **2003**, *42*, 5974; b) M. P. Jensen, M. Costas, R. Y. N. Ho, J. Kaizer, A. Mairata i Payeras, E. Münck, L. Que, Jr., J.-U. Rohde, A. Stubna, *J. Am. Chem. Soc.* **2005**, *127*, 10512; c) M. Martinho, G. Q. Xue, A. T. Fiedler, L. Que, Jr., E. L. Bominaar, E. Münck, *J. Am. Chem. Soc.* **2009**, *131*, 5823.
- [15] M. Martinho, F. Banse, J.-F. Bartoli, T. A. Mattioli, P. Battioni, O. Horner, S. Bourcier, J.-J. Girerd, *Inorg. Chem.* **2005**, *44*, 9592.
- [16] T. K. Paine, M. Costas, J. Kaizer, L. Que, Jr., *J. Biol. Inorg. Chem.* **2006**, *11*, 272.
- [17] J. Yoon, S. A. Wilson, Y. K. Jang, M. S. Seo, K. Nehru, B. Hedman, K. O. Hodgson, E. Bill, E. I. Solomon, W. Nam, *Angew. Chem.* **2009**, *121*, 1283; *Angew. Chem. Int. Ed.* **2009**, *48*, 1257.
- [18] J. Kaizer, E. J. Klinker, N. Y. Oh, J.-U. Rohde, W. J. Song, A. Stubna, J. Kim, E. Münck, W. Nam, L. Que, Jr., *J. Am. Chem. Soc.* **2004**, *126*, 472.
- [19] V. Bolland, M. F. Charlot, F. Banse, J. J. Girerd, T. A. Mattioli, E. Bill, J. F. Bartoli, P. Battioni, D. Mansuy, *Eur. J. Inorg. Chem.* **2004**, 301.
- [20] J. Bautz, M. R. Bukowski, M. Kerscher, A. Stubna, P. Comba, A. Lienke, E. Münck, L. Que, Jr., *Angew. Chem.* **2006**, *118*, 5810; *Angew. Chem. Int. Ed.* **2006**, *45*, 5681.
- [21] M. R. Bukowski, P. Comba, A. Lienke, C. Limberg, C. L. de Laorden, R. Mas-Ballesté, M. Merz, L. Que, Jr., *Angew. Chem.* **2006**, *118*, 3524; *Angew. Chem. Int. Ed.* **2006**, *45*, 3446.
- [22] A. Thibon, J. England, M. Martinho, V. G. Young, Jr., J. R. Frisch, R. Guillot, J.-J. Girerd, E. Münck, L. Que, Jr., F. Banse, *Angew. Chem.* **2008**, *120*, 7172; *Angew. Chem. Int. Ed.* **2008**, *47*, 7064.
- [23] M. R. Bukowski, K. D. Koehntop, A. Stubna, E. L. Bominaar, J. A. Halfen, E. Münck, W. Nam, L. Que, Jr., *Science* **2005**, *310*, 1000.

- [24] J. England, M. Martinho, E. R. Farquhar, J. R. Frisch, E. L. Bominaar, E. Münck, L. Que, Jr., *Angew. Chem.* **2009**, *121*, 3676; *Angew. Chem. Int. Ed.* **2009**, *48*, 3622.
- [25] J. England, Y. Guo, E. R. Farquhar, V. G. Young, Jr., E. Münck, L. Que, Jr., *J. Am. Chem. Soc.* **2010**, *132*, 8635.
- [26] D. C. Lacy, R. Gupta, K. L. Stone, J. Greaves, J. W. Ziller, M. P. Hendrich, A. S. Borovik, *J. Am. Chem. Soc.* **2010**, *132*, 12188.
- [27] E. J. Klinker, J. Kaizer, W. W. Brennessel, N. L. Woodrum, C. J. Cramer, L. Que, Jr., *Angew. Chem.* **2005**, *117*, 3756; *Angew. Chem. Int. Ed.* **2005**, *44*, 3690.
- [28] L. Que Jr., *Acc. Chem. Res.* **2007**, *40*, 493.
- [29] W. Nam, *Acc. Chem. Res.* **2007**, *40*, 522.
- [30] C. V. Sastri, M. S. Seo, M. J. Park, K. M. Kim, W. Nam, *Chem. Commun.* **2005**, 1405.
- [31] M. J. Park, J. Lee, Y. Suh, J. Kim, W. Nam, *J. Am. Chem. Soc.* **2006**, *128*, 2630.
- [32] J. Bautz, P. Comba, C. L. de Laorden, M. Menzel, G. Rajaraman, *Angew. Chem.* **2007**, *119*, 8213; *Angew. Chem. Int. Ed.* **2007**, *46*, 8067.
- [33] N. Y. Oh, Y. Suh, M. J. Park, M. S. Seo, J. Kim, W. Nam, *Angew. Chem.* **2005**, *117*, 4307; *Angew. Chem. Int. Ed.* **2005**, *44*, 4235.
- [34] C. V. Sastri, J. Lee, K. Oh, Y. J. Lee, J. Lee, T. A. Jackson, K. Ray, H. Hirao, W. Shin, J. A. Halfen, J. Kim, L. Que, Jr., S. Shaik, W. Nam, *Proc. Natl. Acad. Sci. USA* **2007**, *104*, 19181.
- [35] P. Comba, S. Fukuzumi, H. Kotani, S. Wunderlich, *Angew. Chem.* **2010**, *122*, 2679; *Angew. Chem. Int. Ed.* **2010**, *49*, 2622.
- [36] W. Nam, *Acc. Chem. Res.* **2007**, *40*, 465.
- [37] S. P. de Visser, K. Oh, A.-R. Han, W. Nam, *Inorg. Chem.* **2007**, *46*, 4632.
- [38] C. V. Sastri, K. Oh, Y. J. Lee, M. S. Seo, W. Shin, W. Nam, *Angew. Chem.* **2006**, *118*, 4096; *Angew. Chem. Int. Ed.* **2006**, *45*, 3992.
- [39] A. R. Ekkati, J. J. Kodanko, *J. Am. Chem. Soc.* **2007**, *129*, 12390.
- [40] A. A. Campanali, T. D. Kwiecien, L. Hryhorczuk, J. J. Kodanko, *Inorg. Chem.* **2010**, *49*, 4759.
- [41] J. Bernadou, B. Meunier, *Chem. Commun.* **1998**, 2167.
- [42] M. D. Wolfe, J. D. Lipscomb, *J. Biol. Chem.* **2003**, *278*, 829.
- [43] K. Chen, L. Que, Jr., *Chem. Commun.* **1999**, 1375.
- [44] M. S. Seo, J.-H. In, S. O. Kim, N. Y. Oh, J. Hong, J. Kim, L. Que, Jr., W. Nam, *Angew. Chem.* **2004**, *116*, 2471; *Angew. Chem. Int. Ed.* **2004**, *43*, 2417.
- [45] A. Company, L. Gómez, M. Güell, X. Ribas, J. M. Luis, L. Que, Jr., M. Costas, *J. Am. Chem. Soc.* **2007**, *129*, 15766.
- [46] C. V. Sastri, M. J. Park, T. Ohta, T. A. Jackson, A. Stubna, M. S. Seo, J. Lee, J. Kim, T. Kitagawa, E. Münck, L. Que, Jr., W. Nam, *J. Am. Chem. Soc.* **2005**, *127*, 12494.
- [47] D. A. Proshlyakov, T. F. Henshaw, G. R. Monterosso, M. J. Ryle, R. P. Hausinger, *J. Am. Chem. Soc.* **2004**, *126*, 1022.
- [48] DFT geometries were optimized at the B3LYP level in conjunction with the SDD basis set and associated ECP for Fe, and the 6-311G-(d,p) basis set was employed for the other atoms, as implemented in the Gaussian 09 program.<sup>[50]</sup> The energies were further refined by single-point calculations with the cc-pVTZ basis set for Fe, and the atoms bonded to Fe, and the cc-pVDZ basis set for the other atoms (B3LYP/cc-pVTZ&cc-pVDZ//B3LYP/SDD&6-311G(d,p)). Final free energies include energies computed at the B3LYP/cc-pVTZ&cc-pVDZ//B3LYP/SDD&6-311G(d,p) level of theory together with enthalpic and free energy corrections at the B3LYP/LANL2DZ&D95V level (i.e., B3LYP level in conjunction with the LANL2DZ basis set and associated ECP for Fe, and D95V basis set for the other atoms).
- [49] Gaussian 09, Revision A.02, M. J. Frisch, G. W. Trucks, H. B. Schlegel, G. E. Scuseria, M. A. Robb, J. R. Cheeseman, G. Scalmani, V. Barone, B. Mennucci, G. A. Petersson, H. Nakatsuji, M. Caricato, X. Li, H. P. Hratchian, A. F. Izmaylov, J. Bloino, G. Zheng, J. L. Sonnenberg, M. Hada, M. Ehara, K. Toyota, R. Fukuda, J. Hasegawa, M. Ishida, T. Nakajima, Y. Honda, O. Kitao, H. Nakai, T. Vreven, J. A. Montgomery, Jr., J. E. Peralta, F. Ogliaro, M. Bearpark, J. J. Heyd, E. Brothers, K. N. Kudin, V. N. Staroverov, R. Kobayashi, J. Normand, K. Raghavachari, A. Rendell, J. C. Burant, S. S. Iyengar, J. Tomasi, M. Cossi, N. Rega, J. M. Millam, M. Klene, J. E. Knox, J. B. Cross, V. Bakken, C. Adamo, J. Jaramillo, R. Gomperts, R. E. Stratmann, O. Yazyev, A. J. Austin, R. Cammi, C. Pomelli, J. W. Ochterski, R. L. Martin, K. Morokuma, V. G. Zakrzewski, G. A. Voth, P. Salvador, J. J. Dannenberg, S. Dapprich, A. D. Daniels, O. Farkas, J. B. Foresman, J. V. Ortiz, J. Cioslowski, and D. J. Fox, Gaussian, Inc., Wallingford CT, **2009**.
- [50] A. Company, L. Gómez, X. Fontrodona, X. Ribas, M. Costas, *Chem. Eur. J.* **2008**, *14*, 5727.
- [51] As above the final free energies include energies computed at the B3LYP/cc-pVTZ&cc-pVDZ//B3LYP/SDD&6-311G(d,p) level of theory together with enthalpic and free energy corrections at the B3LYP/LANL2DZ&D95V level. The cc-pVTZ basis set is also used for the H atoms bound to oxygen.
- [52] J.-U. Rohde, S. Torelli, X. Shan, M. H. Lim, E. J. Klinker, J. Kaizer, K. Chen, W. Nam, L. Que, Jr., *J. Am. Chem. Soc.* **2004**, *126*, 16750.
- [53] P. J. Riggs-Gelasco, J. C. Price, R. B. Guyer, J. H. Brehm, E. W. Barr, J. M. Bollinger, Jr., C. Krebs, *J. Am. Chem. Soc.* **2004**, *126*, 8108.
- [54] D. Galonic Fujimori, E. W. Barr, M. L. Matthews, G. M. Koch, J. R. Yonce, C. T. Walsh, J. Martin Bollinger, Jr., C. Krebs, P. J. Riggs-Gelasco, *J. Am. Chem. Soc.* **2007**, *129*, 13408.
- [55] CCDC-782986 contains the supplementary crystallographic data for this paper. These data can be obtained free of charge from the Cambridge Crystallographic Data Centre via [www.ccdc.cam.ac.uk/data\\_request/cif](http://www.ccdc.cam.ac.uk/data_request/cif).
- [56] K. Chen, L. Que, Jr., *J. Am. Chem. Soc.* **2001**, *123*, 6327.
- [57] H. Erras-Hanauer, T. Clark, R. van Eldik, *Coord. Chem. Rev.* **2003**, *238–239*, 233.
- [58] The final free energies include energies computed at the B3LYP-D3/cc-pVTZ&cc-pVDZ//B3LYP/LANL2DZ&D95V level of theory together with enthalpic and free energy corrections at the B3LYP/LANL2DZ&D95V level (see ref. [48] for more details). The single-point calculations include the acetonitrile solvent effect computed through the Gaussian 09 PCM approach and the London dispersion effects calculated using the Grimme DFT-D3 method.
- [59] S. Miertuš, E. Scrocco, J. Tomasi, *Chem. Phys.* **1981**, *55*, 117.
- [60] S. Grimme, J. Antony, S. Ehrlich, H. Krieg, *J. Chem. Phys.* **2010**, *132*, 154104.
- [61] G. Yin, A. M. Danby, D. Kitko, J. D. Carter, W. M. Scheper, D. H. Busch, *J. Am. Chem. Soc.* **2007**, *129*, 1512.
- [62] P. Comba, G. Rajaraman, *Inorg. Chem.* **2008**, *47*, 78.
- [63] S. O. Kim, C. V. Sastri, M. S. Seo, J. Kim, W. Nam, *J. Am. Chem. Soc.* **2005**, *127*, 4178.
- [64] Y. Goto, T. Matsui, S.-i. Ozaki, Y. Watanabe, S. Fukuzumi, *J. Am. Chem. Soc.* **1999**, *121*, 9497.
- [65] G. Xue, R. D. Hont, E. Münck, L. Que, Jr., *Nat. Chem.* **2010**, *2*, 400.
- [66] C. R. Goldsmith, R. T. Jonas, T. D. P. Stack, *J. Am. Chem. Soc.* **2002**, *124*, 83.
- [67] Y.-R. Luo, *Comprehensive Handbook of Chemical Bond Energies*, CRC Press, Boca Raton, **2007**.
- [68] T. Matsuo, J. M. Mayer, *Inorg. Chem.* **2005**, *44*, 2150.
- [69] J. R. Bryant, J. M. Mayer, *J. Am. Chem. Soc.* **2003**, *125*, 10351.
- [70] C. R. Goldsmith, A. P. Cole, T. D. P. Stack, *J. Am. Chem. Soc.* **2005**, *127*, 9904.
- [71] A. S. Larsen, K. Wang, M. A. Lockwood, G. L. Rice, T.-J. Won, S. Lovell, M. Sadilek, F. Tureek, J. M. Mayer, *J. Am. Chem. Soc.* **2002**, *124*, 10112.
- [72] D. E. Lansky, D. P. Goldberg, *Inorg. Chem.* **2006**, *45*, 5119.
- [73] J. M. Mayer, *Acc. Chem. Res.* **1998**, *31*, 441.
- [74] E. J. Klinker, S. Shaik, H. Hirao, L. Que, Jr., *Angew. Chem.* **2009**, *121*, 1317–1321; *Angew. Chem. Int. Ed.* **2009**, *48*, 1291–1295.
- [75] D. Wang, M. Zhang, P. Bühlmann, L. Que, Jr., *J. Am. Chem. Soc.* **2010**, *132*, 7638.
- [76] C. Fertinger, N. Hessenauer-Ilicheva, A. Franke, R. van Eldik, *Chem. Eur. J.* **2009**, *15*, 13435.
- [77] A. Kohen, J. P. Klinman, *Acc. Chem. Res.* **1998**, *31*, 397.
- [78] Z. Pan, J. H. Horner, M. Newcomb, *J. Am. Chem. Soc.* **2008**, *130*, 7776.

- [79] J. C. Price, E. W. Barr, T. E. Glass, C. Krebs, J. Martin Bollinger, Jr., *J. Am. Chem. Soc.* **2003**, *125*, 13008.
- [80] E. R. Lewis, E. Johansen, T. R. Holman, *J. Am. Chem. Soc.* **1999**, *121*, 1395.
- [81] J. C. Nesheim, J. D. Lipscomb, *Biochemistry* **1996**, *35*, 10240.
- [82] S. Fukuzumi, H. Kotani, Y.-M. Lee, W. Nam, *J. Am. Chem. Soc.* **2008**, *130*, 15134.
- [83] Y. J. Jeong, Y. Kang, A.-R. Han, Y.-M. Lee, H. Kotani, S. Fukuzumi, W. Nam, *Angew. Chem.* **2008**, *120*, 7431; *Angew. Chem. Int. Ed.* **2008**, *47*, 7321.
- [84] C. Arunkumar, Y.-M. Lee, J. Y. Lee, S. Fukuzumi, W. Nam, *Chem. Eur. J.* **2009**, *15*, 11482.
- [85] K. A. Gardner, J. M. Mayer, *Science* **1995**, *269*, 1849.
- [86] G. K. Cook, J. M. Mayer, *J. Am. Chem. Soc.* **1995**, *117*, 7139.
- [87] G. K. Cook, J. M. Mayer, *J. Am. Chem. Soc.* **1994**, *116*, 1855.
- [88] D. Wang, E. R. Farquhar, A. Stubna, E. Münck, L. Que, Jr., *Nat. Chem.* **2009**, *1*, 145.
- [89] A. Gunay, K. H. Theopold, *Chem. Rev.* **2010**, *110*, 1060.
- [90] D. Kumar, H. Hirao, L. Que, Jr., S. Shaik, *J. Am. Chem. Soc.* **2005**, *127*, 8026.
- [91] H. Hirao, D. Kumar, L. Que, Jr., S. Shaik, *J. Am. Chem. Soc.* **2006**, *128*, 8590.
- [92] S. P. De Visser, *J. Am. Chem. Soc.* **2010**, *132*, 1087.
- [93] Y. Zhou, X. Shan, R. Mas-Ballesté, M. R. Bukowski, A. Stubna, M. Chakrabarti, L. Slominski, J. A. Halfen, E. Münck, L. Que, Jr., *Angew. Chem.* **2008**, *120*, 1922–1925; *Angew. Chem. Int. Ed.* **2008**, *47*, 1896–1899.
- [94] a) N. C. Handy, A. J. Cohen, *Mol. Phys.* **2001**, *99*, 403; b) J. P. Perdew, K. Burke, M. Ernzerhof, *Phys. Rev. Lett.* **1996**, *77*, 3865.
- [95] a) A. Klamt, *J. Phys. Chem.* **1995**, *99*, 2224; b) A. Klamt, V. Jonas, *J. Chem. Phys.* **1996**, *105*, 9972; c) A. Klamt, G. Schüürmann, *J. Chem. Soc. Perkin Trans. 2* **1993**, 799.
- [96] E. J. Baerends, J. Autschbach, A. Bérces, J. A. Berger, F. M. Bickelhaupt, C. Bo, P. L. de Boeij, P. M. Boerrigter, L. Cavallo, D. P. Chong, L. Deng, R. M. Dickson, D. E. Ellis, M. van Faassen, L. Fan, T. H. Fischer, C. Fonseca Guerra, S. J. A. van Gisbergen, J. A. Groeneveld, O. V. Gritsenko, M. Grüning, F. E. Harris, P. van den Hoek, C. R. Jacob, H. Jacobsen, L. Jensen, E. S. Kadantsev, G. van Kessel, R. Klooster, F. Kootstra, E. van Lenthe, D. A. McCormack, A. Michalak, J. Neugebauer, V. P. Nicu, V. P. Osinga, S. Patchkovskii, P. H. T. Philipsen, D. Post, C. C. Pye, W. Ravenek, P. Romaniello, P. Ros, P. R. T. Schipper, G. Schreckenbach, J. G. Snijders, M. Solà, M. Swart, D. Swerhone, G. te Velde, P. Vernooijs, L. Versluis, I. Visscher, O. Visser, F. Wang, T. A. Wesolowski, E. M. van Wezenbeek, G. Wiesenekker, S. K. Wolff, T. K. Woo, A. L. Yakovlev, T. Ziegler, ADF 2009.01; SCM, Amsterdam, The Netherlands, **2009**.
- [97] a) W. G. Han, L. Noodleman, *Inorg. Chem.* **2008**, *47*, 2975; b) W. G. Han, T. Q. Liu, T. Lovell, L. Noodleman, *J. Comput. Chem.* **2006**, *27*, 1292; c) W. G. Han, L. Noodleman, *Inorg. Chim. Acta* **2008**, *361*, 973.

Received: August 11, 2010  
Published online: January 5, 2011